Design of a C-band Conformal Phased-Array Antenna for Airborne Synthetic Aperture Radar

Tamás Gál

A thesis submitted in partial fulfillment of the requirements for the degree of

Master of Science

University of Washington

2014

Committee:

Gordon Farquharson

Yasuo Kuga

Jorge L. Salazar-Cerreno

Program Authorized to Offer Degree: Department of Electrical Engineering

University of Washington

Abstract

Design of a C-band Conformal Phased-Array Antenna

for Airborne Synthetic Aperture Radar

Tamás Gál

Chair of the Supervisory Committee:

Professor Gordon Farquharson

Department of Electrical Engineering

The design of an aerodynamically efficient antenna is considered for an airborne synthetic aperture radar (SAR). The requirements for the antenna are derived from the desired performance of the radar, and practical considerations for mounting antennas on a small aircraft. The design and the performance of the antenna is presented.

TABLE OF CONTENTS

LIST OF FIGURES

LIST OF TABLES

ACKNOWLEDGMENTS

First and foremost, I would like to thank Professor Gordon Farquharson for giving me the opportunity to work on this project. Ever since then, he relentlessly supported and encouraged me when I despaired in the face of obstacles that were blocking my research. I could not have asked for a better advisor than Gordon, and I feel very lucky to have been able to work with him.

My co-advisor, Professor Yauso Kuga, introduced me to the world of antennas and patiently guided me through the design process. He taught me antenna measurement techniques and simulation software, which were essential for this project. He also made sure I stayed on track, and gave me practical advise when I needed it the most.

If it had not been for Dr. Jorge L. Salazar-Cerreno at the National Center for Atmospheric Research in Boulder, Colorado, I probably would never have considered aperture-couple patch antennas, which greatly simplified the design and allowed me to create antennas in a timely manner that worked very well in the end. Jorge's synthesis method, his dedication to helping me, his reviews of my design, and his suggestions to improve on the measurements made it possible to make this project a success.

I would also like to express my gratitude to John Mower at the Applied Physics Laboratory at the University of Washington. He helped a lot with the practical aspects of the antenna: the design and fabrication of the connectors, as well as the experimental setup and measurements. In addition, I made extensive use of a software tool he had written to obtain the radiation patterns.

The amount of knowledge I gathered from having worked with Gordon, Professor Kuga, Jorge, and John is the greatest gift anybody could have given me. Thank you all for being a part of my education!

DEDICATION

To

Art, Max, Zs,

and of course

Kitty,

and

Mommy

Chapter 1. Introduction

Radar uses electromagnetic waves to gather information about distant objects. It provides measurement capabilities without physical contact; therefore, it is well suited for remote sensing applications. Initially developed for "radio detection and ranging" for the military in the 1940s, it has since been used in a wide range of disciplines including astronomy, aviation, geology, meteorology, and oceanography.

A critical component of radar is the antenna, which acts as the interface between the outside world (the free-space where electromagnetic waves between the object and the radar propagate) and the internals of the radar (which process the signals).

In this thesis, a purpose-built radar antenna design and its measured characteristics are reported. First, the radar system and its application are described as these govern many aspects of the basic antenna requirements. This is followed by the actual step-by-step design procedure of the new antenna including an investigation of different approaches and explanations of key design decisions. Next, experimental measurements of the manufactured antenna are presented and compared with the expected simulated results. Finally, ways for further improvement based on the findings of this thesis are discussed.

1.1 Motivation

The Applied Physics Laboratory at the University of Washington (APL-UW) has an operational compact synthetic aperture radar (SAR) suitable for a Cessna 172 aircraft. The most visible part of the system are six flat-panel antennas mounted on the bottom of the fuselage (Figure 1.1). This adds extra weight and drag to the aircraft and results in increased fuel consumption and reduced range

by up to 20%. This decrease in aircraft performance would be improved if the current antennas were replaced by conformal antennas mounted on the surface of the aircraft. Aerodynamic drag would be greatly reduced along with the total weight, which would make the operation of the radar more economical. In addition, the new antenna may make it also possible to transfer the entire radar system to an unmanned aerial vehicle (UAV) for further cost savings.

Figure 1.1: The current antennas on the underside of the aircraft

1.2 Radar Application

The radar system is used for remote measurement of near-shore ocean and river surface current velocities. The measurements are made with an airborne side-looking synthetic aperture radar overflying the region to be mapped. Forward and aft squinted radars are used to determine line-of-sight velocity components of the surface waves, which are then combined to estimate the actual velocity vector.

1.2.1 Measurement of Surface Velocity

Simple radar operating on the principle of measuring the time elapsed between a signal sent and its reflection received can only measure distances. Measurement of velocity is based on the Doppler effect, i.e. the frequency shift of the signal as it is reflected from a moving object. An electromagnetic wave of frequency f_{tx} reflecting from object with a velocity v in the direction of the wave propagation will have a frequency of

$$f_{rx} = f_{tx}\left(\frac{1+\frac{v}{c}}{1-\frac{v}{c}}\right) \tag{1.1}$$

The Doppler-shift is the change in frequency, and as such is given by

$$f_D = f_{rx} - f_{tx} = 2v\left(\frac{f_{tx}}{c-v}\right) \approx 2v\frac{f_{tx}}{c} \quad for \quad v \ll c \tag{1.2}$$

A Doppler radar measures this frequency difference between the transmitted and received signals. From this, the line-of-sight velocity of the object from which the signal was reflected can be calculated.

The restoring force for ocean waves are dominated by two mechanisms: one is gravity, the other is surface tension. The former is responsible for high-energy and low-frequency waves present in a thick layer of water, whereas the letter normally causes high-frequency surface waves only [1]. This makes the surface of the water to be rough, from which the incident electromagnetic wave undergoes diffuse scattering. This affects the amount and polarity of the wave returned to the radar, which will be discussed in more detail in Section 1.3.3.

1.2.2 Dual-Beam Along-Track Interferometry

A synthetic aperture radar uses the Doppler shift between the aircraft and the surface to position scatterers in the cross-range dimension. Along-track interferometry is a method through which the mean Doppler shift is measured by a synthetic aperture radar. The amount of Doppler shift mea-

sured is directly proportional to the line-of-sight velocity component of the scatterer. Therefore, in order to recover surface velocity, two components of the velocity vector need to be measured. These components should be orthogonal, or as close to orthogonal as practical. With a single aircraft, this can be done by using two side-looking radars; one forward and one aft. While it does take some time for the two radars to map the same surface, experiments have shown satisfying results [2].

1.2.3 Airborne Systems

Integrating a radar with an aircraft depends mainly on the size and weight of both. A larger radar system needs a larger aircraft to be able to host and carry it. In turn, the size of the aircraft exclusively drives the operating costs of the radar. Fuel prices and aircraft and pilot rental fees rise sharply with larger aircraft. In 2002, operating a radar system designed differently but for a similar application as the one outlined in this thesis on a Lockheed P-3 aircraft (with a maximum useful load of approx. 26,000 kg) [3] cost several thousand USD per hour. Compared to this is the few hundred USD per hour operating cost on a Cessna 172 aircraft (with a 400 kg useful load).

Because of this, there is strong financial incentive to miniaturize radar systems, which are now of sufficiently small size and weight that putting them on a UAV is feasible. While the main goal of this project was to create new antennas to replace the current ones and to continue to operate the system on the Cessna 172 aircraft, the aim is also to investigate whether sufficient reduction is size, weight and induced aerodynamic drag can be achieved to make it possible to integrate the system with a UAV.

1.3 System Description

The antenna requirements are closely tied to how the radar operates. For this reason, the components and key design decisions of the radar system will be reviewed in detail in the following sections.

1.3.1 Size & Weight

A Cessna 172 aircraft has a useful load of 400 kg*. This includes fuel, the pilot, any additional passengers, and payload. The aircraft can hold 150 liters* of aviation fuel which has mass of 120 kg*. Adding an 80 kg* pilot and an 80 kg* passenger to operate the radar leaves 120 kg* for the entire radar system, which also needs to fit in a space comparable to that of a small 4-seater passenger car and corresponding baggage compartment (not including the antenna). Therefore, it is essential to keep the size and weight of the system at a minimum.

Figure 1.2: The Cessna 172S aircraft used in our experiments

1.3.2 Power & Type of Radar

The amplifier used in the APL-UW system is a 1 W amplifier because a larger power source would require special cooling mechanism, adding to the weight, complexity and size of the system. With low power it is essential that the average power output is maximized for sufficient signal-to-noise ratio to make a good measurement. For this reason a Continuous Wave (CW) radar is used instead of pulse radar. CW radar works by continuously transmitting the signal; therefore, it requires both a transmitting and receiving antenna. The addition of a second antenna has implications for the size of the antennas. Furthermore, regular CW radars can only be used for velocity measurements

*Approximate values

based on the Doppler-shift of the frequency reflected from the target. They are not suited to make distance measurements, since they are missing a time reference. To rectify this, the CW pulse is modulated to create a Frequency Modulated Continuous Wave (FMCW) radar. FMCW radar changes the frequency of the emitted signal linearly with time between two predefined values periodically. In this way, both radial velocity and distance can be recovered from the received signal.

1.3.3 Frequency

The frequency band to be used is a compromise between several theoretical considerations and engineering requirements, which may favor higher or lower frequencies.

In order to receive reflected EM-waves from the ocean surface, it has to be a rough surface as defined by the Raleigh criterion:

$$\frac{\lambda}{8 \cdot \cos\theta} < h \tag{1.3}$$

where λ is the radar wavelength, θ is the incident angle and h is the mean height of surface variation.

In addition, the strength of the scattering is determined by the Bragg scattering [4], where the Bragg-resonant wavelength is given by

$$\Lambda = \frac{\lambda}{2 \cdot \sin\theta} \tag{1.4}$$

where Λ is the ocean surface wavelength, λ is the radar wavelength, and θ is the incident angle. In general, the strength of the scattering from the ocean surface in the microwave regime is larger for longer electromagnetic waves [5].

From an engineering perspective, the antenna beam width is generally related to the wavelength and the physical size of the antenna by

$$\theta_W \approx \frac{\lambda}{D} \tag{1.5}$$

where θ_W is the beam width, λ is the radar wavelength, and D is the size of the antenna. From this, one can see that in order to keep a constant beam width a larger wavelength would require a larger antenna.

While L-band (1-2 GHz) is a good choice in terms of scattering length, antennas at this frequency are large, and therefore not suitable for small aircraft. In addition, it is difficult to achieve a large operating bandwidth (200 MHz at 1 GHz center) at these frequencies. X-band (8-10 GHz) enables smaller antennas, but the decorrelation time of the surface (the time in which scattering from the surface can be coherently averaged to improve signal-to-noise ratio) is around 50 ms, or half of the decorrelation time for C-band (4-8 GHz) [2]. This limits the maximum distance between antennas and results in lower resolution (discussed in detail in Section 1.3.7). For a small aircraft with a limited top speed of around 100 knots C-band is a good compromise between antenna size and decorrelation time. In particular, the amplifier in our system emits signals between 5328.76 MHz and 5528.76 MHz.

1.3.4 Bandwidth

Two components of the surface velocity need to be measured, which necessitates the use of two separate radar systems oriented in a non-parallel direction with respect to each other. Hence, one is oriented forward and the other backwards for along-track illumination. As the antennas have to be placed in close proximity to each other, the 200 MHz bandwidth output of the amplifier is split into a lower and upper 80 MHz sections with an unused 40 MHz in between for avoiding interference. This is illustrated in Table 1.1.

There are two obvious approaches to designing antennas for this application: one is to create one antenna that works in the required frequency ranges of both radars (option 1), and the other is to have two with characteristics optimized for each (option 2). The former requires the antenna to have a bandwidth of 200 MHz or roughly 3.8%, whereas the latter design approach would result

Table 1.1: Operating radar frequency ranges

Radar 1	5328.76 - 5408.76 MHz
Guard band	5408.76 - 5448.76 MHz
Radar 2	5448.76 - 5528.76 MHz

in a lower bandwidth requirement of 80 MHz or 1.5%. While it is easier to achieve the lower bandwidth, the goal is to create identical and interchangeable antennas. Therefore, an antenna design with a center frequency of 5.43 GHz and bandwidth of somewhat higher than 200 MHz will be attempted.

1.3.5 Polarization

From the rough ocean surface, the vertically polarized waves scatter more efficiently than horizontally polarized waves for high incident angles. Therefore, in order to maximize reflection from the ocean surface, the transmitted wave should be perpendicularly polarized. The reflected wave will have the same polarization, which allows us to use identical antennas for transmission and detection.

1.3.6 Radiation Pattern

For cross-track illumination, a compromise between maximum range and high incident angles is needed. Looking further to the side also requires a higher gain for the antenna, but looking more vertically down would increase the contribution of the vertical component of the velocity in the Doppler shift. Since the horizontal flow of the water is to be measured, the vertical component should be minimized. A compromise between these two requirements is met by the current system using 60° vertical incidence with 30° beam width.

The horizontal squinting of the antennas is required to ensure that the two radar set measurements contain orthogonal components of the ocean surface velocities. Since the conformal antennas are to be attached to the fuselage along its side, they will also be parallel to the direction of

travel of the aircraft, thereby making simple broadside antennas only be able to look perpendicular to the line of travel. While a 45° squinting would ensure orthogonality, this is not necessary to make good measurements. In the current setup, the mechanically aligned antennas are squinted at ±30°. For the electronically squinted antennas 25° squint is sought as it would also decrease the time between illumination of the same area by the forward and aft-looking radars.

In order to make statistically independent measurements of the individual scatterers on the ground, the area illumination time needs to be long enough compared to the de-correlation time of the area. Therefore, this imposes a lower limit on the beam width. The de-correlation time of the ocean surface is about 50 ms at 10 GHz, and 100 ms at 5 GHz. The number of possible independent measurements is then given by as the ratio of the area illumination time and the de-correlation time. In our case, the goal is to make at least 10 independent measurements, or a minimum of 1 s area illumination time. With simple geometry one can show that a few degrees of horizontal beam width is sufficient for these purposes. The current system has a 7° beam width, but in order to ensure a high antenna gain, a 5° beam width will be sought.

1.3.7 Resolution

The primary application of this radar is to measure the velocity of ocean currents. This means identifying masses of water with particles having relatively uniform velocities surrounded by a larger body of water with non-uniform particle velocities. Ocean currents may extend from hundreds of meters to hundreds of kilometers; therefore, a resolution of the order of several meters is sufficient for our purposes.

As it will be described in the next section, the resolution affects the antenna design by establishing a minimum gain requirement. Therefore, both the cross-range and azimuth resolutions need to be derived. The former is directly related to the bandwidth B of the antenna (where B = 80 MHz for one direction) as follows:

$$\Delta R = \frac{c}{2B} \approx 1.9\ m \tag{1.6}$$

Azimuth resolution, on the other hand, depends on other factors that are the result of the surface motion and coherence of the scatterers [2]. Neglecting the small effect of surface accelerations, the azimuth resolution is given by

$$\rho_a \approx \sqrt{\left(\frac{\lambda R}{2v_p T_i}\right)^2 + \left(\frac{\lambda R}{2v_p \tau_s}\right)^2} \tag{1.7}$$

where v_p is the platform velocity, T_i is the integration time, and τ_s is the coherence time. The platform velocity is the velocity of the aircraft with respect to the ground, which is approximately 90 knots = 45 m/s. The coherence time depends on frequency and the wind speed [2], and in our case can be approximated to be 100 ms. The integration time is the amount of time a single scatterer is illuminated by the radar beam of width Θ_W as the aircraft flies by it.

$$T_i = \frac{X}{v_p} = \frac{2R\tan\frac{\Theta_W}{2}}{v_p} \approx \frac{R\tan\Theta_W}{v_p} \quad for\ small \quad \Theta_W \tag{1.8}$$

This in our case evaluates to about 3 s, which is much larger than the coherence time. Therefore, Equation 1.7 can be further simplified and evaluated as

$$\rho_a \approx \frac{\lambda R}{2v_p \tau_s} \approx 8.3\ m \tag{1.9}$$

1.3.8 Gain

The radar equation for monostatic radar is given by [6]:

$$P_r = \frac{P_t G^2 \lambda^2 \sigma}{(4\pi)^3 R^4} \tag{1.10}$$

A minimal value of the gain G needs to be determined, which results in a reflected power P_r large enough for detection for given transmitted power P_t, wavelength λ, distance R, and radar cross-section σ. Rearranging Equation 1.10, it becomes:

$$G = \sqrt{\frac{P_r(4\pi)^3 R^4}{P_t \lambda^2 \sigma}} \tag{1.11}$$

The reflected power has to be at least the minimum detectable signal, which is given by

$$P_{min} = kTN_{BW}N_f S_{min} \tag{1.12}$$

where k is the Boltzmann constant, T is the temperature, N_{BW} is the noise bandwidth, N_f is the noise factor and S_{min} is the minimum signal-to-noise ratio needed at the receiver. In addition, the scattering cross-section for the ocean surface is usually defined by an average cross-section per unit area times the area illuminated by the radar, or $\sigma = \sigma^0 A$. Substituting this and the requirement that $P_r \geq P_{min}$ along with Equation 1.12 into Equation 1.11 yields the lower limit on the antenna gain as:

$$G \geq \left(\frac{kTN_{BW}N_f S_{min}(4\pi)^3 R^4}{P_t \lambda^2 \sigma^0 A} \right)^{\frac{1}{2}} \tag{1.13}$$

In this expression P_t = 1 W, λ = 0.05 m, T = 300 K, and R = 1500 m (for radar at 2500 ft = 750 m above ground looking at 60° elevation). S_{min} should be at least 0 dB, and the noise factor is estimated to be N_f = 3.5 dB. The noise bandwidth of the receiver is determined by the chirp length of the frequency modulated signal, which results in an effective pulse repetition frequency and N_{BW} = 750 Hz. The average scattering cross-section of the ocean is estimated as σ^0 = -25 dB [4]. The area illuminated by the beam can be calculated as the product of the cross-range resolution and the azimuth resolution, which were discussed in the previous section. Thus, the area is given by $A = \Delta R \times \rho_a \approx 16\ m^2$. Substituting these values into Equation 1.13 results in a minimum gain requirement of approximately 14 dB. However, this is the minimum gain needed to make good measurements in the bore-sight elevation direction only. Since in the cross-range dimension an area of length 1-2 km is to be measured, the antenna gain needs to be large enough to measure scattering from particles that are further away in range and which are illuminated by an off-center part of the main beam. A radial deviation of 1000 m from the bore-sight 60° elevation increases

the range to about 2400 m, which now requires the antenna to have a minimum gain of 18 dB at 72°. Therefore, a minimum gain of about 18 dB or larger is desired with a wide beam width in the elevation plane.

1.3.9 Side Lobes

Since at least two antennas are used in close proximity to each other, care should be taken to avoid unwanted interference from the transmitting antenna to the receiving antenna(s). Side lobes also affect the pulse repetition rate (PRR). Energy measured through the side lobes will have a large Doppler shift, so if the PRR is too low, this energy will be aliased, and will appear at the incorrect cross-range position (ghost images in SAR). Therefore, the side lobe gains should not be more than -20 dB when normalized to the main lobe.

1.3.10 Antenna Size and Placement

As mentioned before, maximizing the average-to-peak transmitted power ratio in the CW radar requires the addition of a secondary receiving antenna to ensure continuous operation for the transmitter. In fact, two antennas are used to receive while one transmits, resulting in three antennas per radar. Each radar uses three antennas, which at present are flat-panel antennas mechanically oriented at pre-determined (fixed) directions. An individual antenna measures 0.2 m x 0.5 m and weighs 3 kg. These antennas have to be placed physically close to each other due to the limited space on the underside of the aircraft fuselage. And since the antennas are mechanically oriented in the desired beam direction, care must be taken to ensure that the interference from the transmitted signal at the receiving antenna is minimized, meaning that at the very least the antennas should not overlap when viewed from the direction of propagation. This puts a lower limit on the distance between the antennas which in turn forces the configuration of the antennas to be Transmitter-Receiver-Receiver, which is not the optimal configuration. Using conformal antennas, it is believed that they can be placed closer to one another, and the system can be operated in a Receiver-Transmitter-Receiver configuration reducing measurement errors.

1.3.11 Mounting

The antenna will be placed on the outside of the aircraft. Since the fuselage is non-uniform along its side, a horizontal cylindrical mount will be affixed to the lower outside section to which the antennas can be attached. This simplifies the design ensuring that the antennas can remain identical. The total available length for the mount is 1.8 m. Eventually there needs to be 6 antennas on this mount. If the arrangement was side-by-side, the maximum length of a single antenna would be 0.3 m. However, placing the forward and aft squinted antennas vertically next to each other doubles the maximum length of an antenna to 0.6 m. On the other hand, the width of the antenna is less constrained, but the aim should still be to minimize the size while ensuring adequate antenna characteristics.

1.3.12 Limitations of the Current System

The entire radar system weighs about 60 kg including the two transceivers, the inertial navigation system (INS), and the six antennas. The volume occupied by the components that are inside the aircraft is about 0.5 m x 0.5 m x 0.5 m weighing 20 kg. In contrast, the antennas and the mount occupy a volume of approximately 1 m x 2 m x 0.3 m and weigh 40 kg. Clearly, in order to further minimize the size and weight of the system to enable it for integration with a UAV, the antennas should be redesigned.

1.4 Antenna Requirements

In the previous sections the various aspects of the radar system for which the antennas are to be developed were discussed. These resulted in specific antenna requirements, which are summarized in the following table.

Table 1.2: Antenna requirements

Frequency range lower	5328.76 - 5408.76 MHz
Frequency range upper	5448.76 - 5528.76 MHz
Bandwidth	200 MHz, 3.7%
Center frequency	5.43 GHz
Polarization	Perpendicular (VV)
Gain	18 dBi
Maximum antenna width	0.6 m
Reference antenna size	0.5 m x 0.2 m
Power	1 W (continuous)
Impedance	50 Ω
Connection	Standard SMA coaxial 50 Ω
Conformity	Horizontally oriented cylindrical (or other smooth surface) mount
Elevation incidence	60° (combination of mechanical and electrical steering)
Elevation beam width	40-50°
Azimuth squint	fixed ±25°
Azimuth beam width	5°

Chapter 2. Background

The design of the antenna begins with a review of previous work. There are lots of different approaches to antenna design, each with its advantages and drawbacks that have to be carefully weighed against each other to best fulfill the operating requirements. Also, antennas are usually not standalone units, in the sense that they are parts of a remote communication or sensing system. Therefore, the antenna design engineer has to keep in mind how the final product will integrate with the rest of the system.

2.1 Microstrip Antennas

Antennas which consist of a radiating element on a grounded dielectric substrate are called microstrip or patch antennas. The advantages of these antennas include their low profile, lightweight construction, a variety of different excitation techniques, and polarization control. Since they are usually fabricated on Printed Circuit Boards (PCBs), this also makes them low-cost for high-scale manufacturing, and suited for integration with printed circuits. On the other hand, patch antennas usually suffer from low bandwidth to center frequency ratios, and the thinness of the microstrip circuit tends to limit their power handling capabilities. As such, these antennas are not suited for wide-band or high-powered applications.

Descriptions and design methodologies of the various kinds of patch antennas which have been considered for this thesis can be found in the following references:

- General discussion on microstrip antennas: [7], [8] and [9]

- Electromagnetically-coupled patch antennas: [10] and [11]
- Aperture-coupled patch antennas: [12], [13], [14], [15] and [16]

2.2 Phased-Array Antennas

Single patch antennas radiate broadside, i.e. in the direction they are facing. Steering the beam of these antennas can be achieved by placing several of them in a row (an array) and introducing a phase difference between them. [8] and [9] give an overview of phased-array antennas, while [17] and [11] describe the design of different phased array antennas.

Phased-array antennas can also be active or passive. An active phased array antenna is electronically steered, i.e. the beam direction can be changed dynamically. This can be achieved by circuitry that changes the phase difference between the radiating elements in response to some control input. On the other hand, a passive phased-array antenna is electronically squinted, meaning it has a fixed beam direction relative to the antenna. If the beam direction is to be changed, then these antennas need to be mechanically oriented. In this thesis, the latter type of antenna design is presented, since the beam direction is fixed with respect to the aircraft, as required for dual-beam interferometric measurements.

2.3 Conformal Antennas

It has already been discussed that the current antenna system increases aerodynamic drag and reduces fuel economy. Conformal antennas offer a remedy to this drawback by conforming to the shape of the object they are attached to. These antennas are mostly used in aerial systems [18]. When changing the shape of an antenna, the radiation pattern and other characteristics may also change, which need to be taken into account. [19] and [20] also describe conformal antennas and design procedures in detail.

In the case of the antennas presented in this thesis, the conformality is going to be limited to a curvature of about 20-25 cm in radius in the elevation plane. This range of values corresponds to

the curvature of the fuselage for a small aircraft or UAV. Therefore, the elevation beam pattern may show some amount of change as the normal angles to the different rows of the antenna increase slightly from being parallel to one another. This depends on the curvature as well as the distance between the rows. The patch sizes and the distances between patches are expected to be in the order of a few cm, thus the curvature will not displace the geometry of the layout by more than a few mm. It is to be seen whether this change will result in any measurable difference in radiation pattern between the flat and the conformal antennas. Moreover, the curvature is not expected to affect the horizontal beam pattern, since the antenna is not bent in the horizontal plane.

Conformal antennas may be fabricated in the final shape, or if the material and design allows for it, they may also be bent after manufactured to a non-conformal shape. In this thesis, the latter will be attempted, partially in order to keep manufacturing costs down, and also to characterize the effects of bending on the flat-panel phased-array antenna.

Chapter 3. Antenna Design

The goal is to create an antenna which conforms to the outer skin of a small aircraft. While the surface of the test airplane is complex, a cylindrical mount will be added to the fuselage to help make the design identical for the six antennas. The mount should still roughly cover the general shape of the fuselage; therefore, its radius should be between 0.2 m and 0.5 m. Since the antenna needs to be thin to minimize the added aerodynamic drag, a microstrip patch array antenna (MSAA) design is considered. MSAAs are also flexible, which is essential for a conformal antenna, and they are cost-effective to manufacture with high-precision printed circuit board (PCB) techniques. The design approach is to use a 2-dimensional array of patch antennas with appropriate placement, phase-shifting, and power tapering to achieve the desired antenna characteristics. Due to the computational complexity of the electromagnetic properties of MSAAs, software tools must be used to design the antennas and to simulate their expected radiation characteristics. For this thesis, Ansoft HFSS and Ansoft Designer were used for modeling and simulations.

There are several factors influencing key decisions about the appropriate design. These will be discussed first in the next section followed by the detailed design of two antennas based on different patch antenna architectures.

3.1 General Considerations

First, the substrate material is chosen since it directly affects the radiating characteristics of the patch antenna, and any computer simulation needs the substrate specified. Then, the cover material is considered, since the radiating copper element should be protected from mechanical and chemical effects. The cover, too, needs to be part of the simulation to ensure reliable results. The

next step is to decide on the type of patch antenna architecture, i.e. how the radiating element will be excited. Once the single element is designed, it is then extended into an array to get the required beam widths and directions in both the elevation and azimuth planes. The feeding network will then have to be designed for proper excitation of the patches. Side lobes and gain are then fine-tuned with power tapering along the array. Finally, the signal connection is considered as it affects manufacturing and assembly.

3.1.1 Substrate

For a given layout the flexibility of the antenna is determined by the thickness and the tensile modulus of the dielectric used in the PCB. It would be tempting to use the thinnest available boards, but the bandwidth of patch antennas in general decreases with thinner boards. Therefore, the boards cannot be arbitrarily thin, and the required radiation characteristics will place a lower limit on the thickness. In addition, the permittivity of the PCB also affects the bandwidth. Using materials with higher dielectric constant leads to lower bandwidth, which means that the same bandwidth can be achieved using a thinner material with lower permittivity. In conclusion, a good choice for a PCB material would be one that has low dielectric constant and low tensile modulus. Low loss tangent is also preferable to maximize efficiency. Table 3.1 summarizes some commercially available PCB materials and their relevant characteristics.

Table 3.1: Dielectric and elastic properties of commercially available PCBs

PCB	ε_r	tan δ	Tensile Modulus
Rogers RT/duroid 5870	2.33	0.0012	1300 MPa at 23°C
Rogers RT/duroid 5880	2.20	0.0009	1070 MPa at 23°C
Rogers RT/duroid 5880LZ	1.96	0.002	n/a
Rogers RT/duroid 6002	2.94	0.0012	828 MPa at 23°C
Rogers RT/duroid 6006	6.45	0.0027	627 MPa at 23°C
Rogers RT/duroid 6010.2LM	10.7	0.0023	931 MPa at 23°C
FR-4 (typical)	4.8	0.017	24 GPa

The material with the best combination of low dielectric constant, low loss tangent and low elasticity was determined to be Duroid 5880. Samples with various thicknesses were ordered from the manufacturer and tested to ensure sufficient flexibility. (While Duroid 5880LZ has the lowest dielectric constant, it is not elastic and so it is not suitable for a conformal antenna.)

3.1.2 PCB Size

The Duroid 5880 PCB comes in standard panel size from 18" x 12" up to 18" x 48". The goal is to make the antennas to be about 0.5 m in length to ensure enough space is available on the aircraft fuselage for three of them. The 2 x 16 configuration discussed previously fits onto a 18" x 24" standard panel. However, when PCB manufacturers were contacted to ensure their capability of making the antenna, all but one (Cirexx International) indicated that the maximum linear size of the boards they can manufacture is 22". Their machinery works on boards up to 24", but the process needs 1" around the edges for tooling which is not available for the end product. Cirexx did offer a 24" long completed board cut from the next bigger sized panel, but their estimated cost was significantly higher (an increase by 40%) than that for 22".

Because of this, the antenna length was maximized at 22", which limited the number of elements that could be used in the array. Two obvious ways of ensuring that the array fits on the smaller board are either to reduce the spacing between adjacent patches, or two reduce the number of patches. The former has the drawback of increasing mutual coupling unless the patch widths are also reduced. Therefore, the latter option was selected, and the array layout was finalized at 2 x 15 elements. The reduced antenna size was expected to increase the beam width, but it was understood to be an acceptable cost-saving measure.

3.1.3 Adhesive

The different PCB layers of the antenna need to be laminated together. This process uses either glue or some special bond ply material. In either case the adhesive affects the radiation characteristics to some extent. As such, it is preferred to know what material will be used and at what thickness

in order to include it in the simulation.

The thickness of glue would be hard to control and apply evenly. Therefore, it was decided to use a Rogers 2929 Bondply material. The manufacturer suggested to use 3 mil of this adhesive for best results.

3.1.4 Cover

The radiating elements of the antenna need to be protected from corrosion and mechanical damage. This necessitates the addition of a cover, which should be low-cost, easily conformable and cause minimal attenuation. Therefore, it was decided that a thin dielectric will be attached to the radiating side of the patch antenna. In this case, however, the close proximity of the dielectric affects the electromagnetic field around the patches, so this extra layer needs to be included in the design simulation. An other approach which does not put the radome in contact with the patches would make the simulation simpler, but the addition of spacers and an air gap would result in a much thicker antenna and more complicated manufacturing process.

High-density polyethylene (HDPE) was initially considered to be used for cover. A 15 mil thick 47" x 120" sheet was obtained for less than 50 USD from a manufacturer for testing purposes. However, the electric characteristics of this material are in general not measured by manufacturers, and they may change across samples manufactured at different times. Therefore, an experimental measurement of the dielectric constant of the test material was carried out. Appendix A describes the measurement procedure and the experimental results in detail. To summarize, the dielectric constant and loss tangent of HDPE could only be determined with a prohibitively high margin of error. As such, the conclusion of the experiment was that HDPE is not a good material to be used in this case regardless of its cost.

With the idea of an inexpensive plastic cover abandoned, the natural choice to consider is the same substrate material as is used in the PCB itself, i.e. Duroid 5880. In addition to its known electrical characteristics, it has the added benefit of having the same thermal properties as the rest of the antenna. This is important to ensure the different layers expand and contract at the same

rate with changing operating temperatures. The thickness of the cover was lowered to 10 mil in an attempt to keep the added attenuation and increased rigidity at a minimum.

3.1.5 Radiating Element

When designing the radiating element of the array, careful consideration needs to be given to how the patch will be excited by the feed line. The various methods give rise to different types of patch antennas including edge-fed, electromagnetically-coupled, and aperture-coupled patch antennas (among others). These differ in their radiation characteristics as well as in their layout, which affects both design and manufacturing complexity. A simple edge-fed patch antenna can be created on a single PCB giving it the lowest manufacturing cost. However, edge-fed patch antennas suffer from low bandwidths of 1-2% [10], which can only be increased with a larger resonating volume. Unfortunately, increasing the patch width or using thick substrates quickly becomes impractical. Furthermore, the feeding network of an edge-fed patch antenna is exposed on the same layer as the radiating patch resulting in unwanted interference in the radiation pattern. For these reasons, this type of antenna is not considered in this design.

There are different ways to increase the bandwidth of patch antennas which excite the patch from another layer thereby also removing the feed line from the radiating surface. One is the probe-fed patch antenna, which adds metal connection across the dielectric separating the patch and the feed using a via. On one hand, vias increase manufacturing complexity and cost, and on the other hand, they are not well-suited for applications where the board is bent. The other approach to excite the patch from a different layer is done by letting the electromagnetic field couple to the patch through the dielectric. There are two well-understood and widely-used types of these, which will be examined in detail: the electromagnetically-coupled and the aperture-coupled patch antennas (EMCPA [10] and ACPA [12]). The way these antennas work will be explained in detail in sections 3.2 and 3.3.

3.1.6 Stack-up

The stack-up refers to the layers of materials that make up the antenna. It is dictated primarily by the architecture (i.e. the way the patch is excited) and also by other considerations such as shielding and placement away from structures interfering with the radiation. The differences between the stack-up of an edge-fed patch antenna, an EMCPA, and an ACPA are illustrated in Figure 3.1.

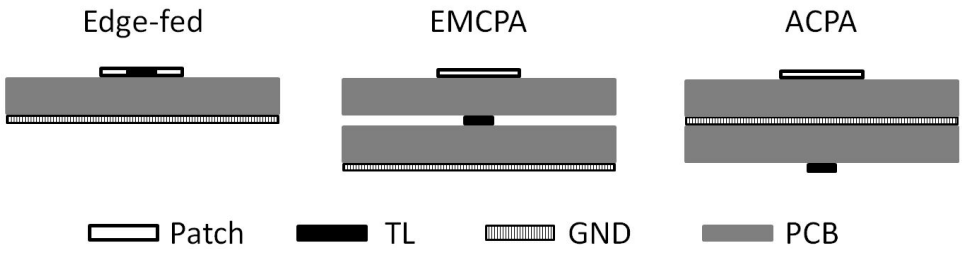

Figure 3.1: Stack-ups of common patch antennas

On one hand, regardless of the architecture chosen, the cover needs to be added on top of the patch layer, slightly increasing the thickness and adding manufacturing cost. On the other hand, the edge-fed and EM-coupled antennas both have the ground plane on the bottom of the stack-up. This is ideal, since this allows direct attachment of the antenna to any surfaces without the need of spacers. The ACPA as shown; however, exposes the feed line on the bottom layer, which is not desired. Therefore, a stripline TL is introduced for the ACPA. Figure 3.9 shows the resulting stack-up, which introduces yet another substrate layer. Whether this increase in complexity and cost is justified will be addressed in sections 3.2 and 3.3 when design based on the different types of excitations are detailed.

3.1.7 Phased Array

Once a suitable radiating element is designed, the next step is to find an array configuration which gives satisfactory beam characteristics (direction and width). For a linear array of isotropic elements, the relationship of the main beam direction (Θ), the distance between the elements (d), the wavelength (λ) and the phase difference ($\Delta\phi$) is given by Equation 3.1.

$$\frac{\Delta\phi}{360^\circ} = \frac{d\sin\Theta}{\lambda} \tag{3.1}$$

This formula can be derived from the geometry illustrated in Figure 3.2. The direction in which the radiation from an array of linearly placed uniform antennas undergoes constructive interference is determined by the amount of extra path length the wave needs to travel to be in phase with the wave from the adjacent antenna.

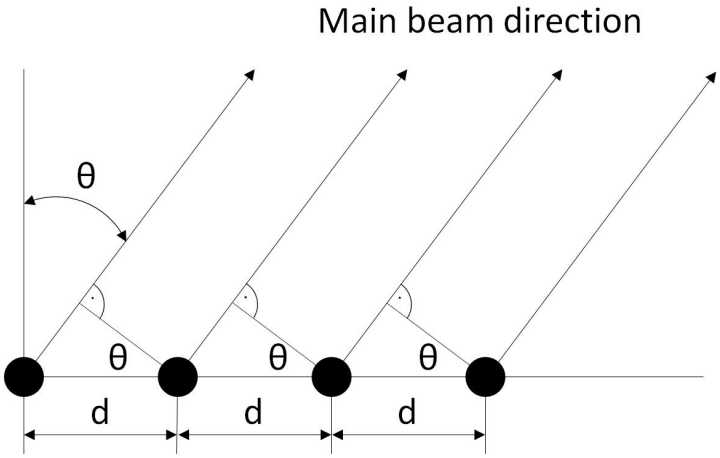

Figure 3.2: Geometric explanation of the array-steer equation

Using the simulated radiation pattern of a single patch, Equation 3.1 and the Ansoft HFSS software were used to calculate the resulting beam pattern in various array configurations. Originally, it was found that with an array of 2 by 16 patches, a satisfactory beam pattern may be obtained (Figure 3.3). Details of the array layout and the simulation results are summarized in Table 3.2. However, the cost of PCB manufacturing eventually limited the size of the board resulting in a reduced number of elements in the final design.

3.1.8 Power Tapering

The uniformly excited antenna array has a theoretical peak side lobe level of -12 dB. This increases illuminating and detecting objects off to the side of the beam direction resulting in unwanted interference. To reduce this, -20 dB side lobes are desired, which can be achieved by varying the

Table 3.2: 2 x 16 phased array layout and calculated beam characteristics

Number of cells in the X direction	16
Number of cells in the Y direction	2
Distance (center-to-center) between cells, X direction	35 mm
Distance (center-to-center) between cells, Y direction	30 mm
Phase shift between adjacent cells, X direction	96°
Phase shift between adjacent cells, Y direction	0°
Beam direction, $\phi = 90°$	25°
Beam width, $\phi = 90°$	5°
Beam direction, $\phi = 0°$	0°
Beam width, $\phi = 0°$	45°

amount of power the patches radiate. A -20 dB Taylor power taper will be applied to the array design by adjusting the impedance of the patches.

3.1.9 Series- vs Corporate-Fed Arrays

The feeding network needs to excite the patches in a precise manner to ensure correct phase differences between the patches and correct power delivered to each of them. The difference between a series and corporate-fed array is illustrated in Figure 3.4. In a series-fed system there are no junctions and no need for impedance matching transfomers, and the distance the signal travels is less than in a corporate-fed system. This makes series-fed networks more efficient and also smaller in size. On the other hand, the design of these networks is more complex, as the magnitude and phase of the impedance have to be carefully calculated as it propagates down the line and changes at every radiating element. In a corporate-fed network, the electrical distance and thus the signal phase and magnitude from the source to the radiating element is the same for all elements. These considerations will have to be weighted against one another when designing the feeding network.

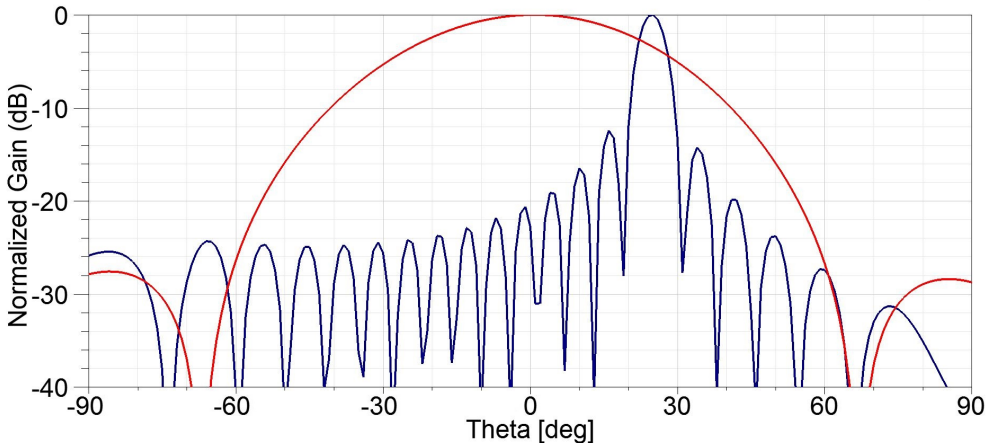

Figure 3.3: Calculated radiation pattern of a 2 x 16 phased array antenna

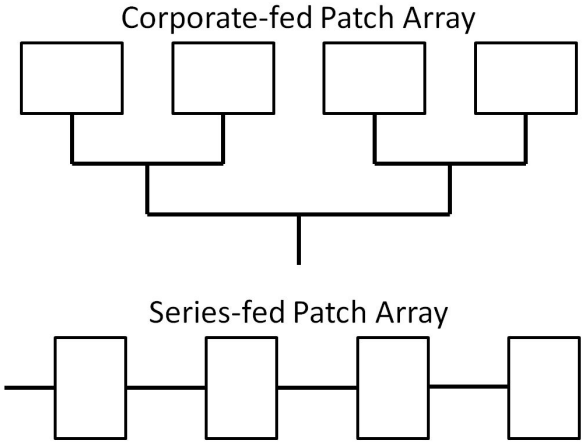

Figure 3.4: Corporate- and series-fed networks

3.2 Electromagnetically-Coupled Patch Antenna Array

The first design approach used an EMCPA for its simplicity. It contains only one extra layer of PCB compared to an edge-fed patch antenna, and the design steps for creating a unit cell radiating at the desired frequency are fairly straightforward. Furthermore, bandwidths up to 10% may be achieved with this layout [10]. EMCPAs eliminate the unwanted interference from the feeding network of an edge-fed patch antenna by inserting a second substrate between the microstrip feed line and the radiating patch and by letting the electromagnetic field couple between the two. The layout of an EMCPA is shown in Figure 3.5.

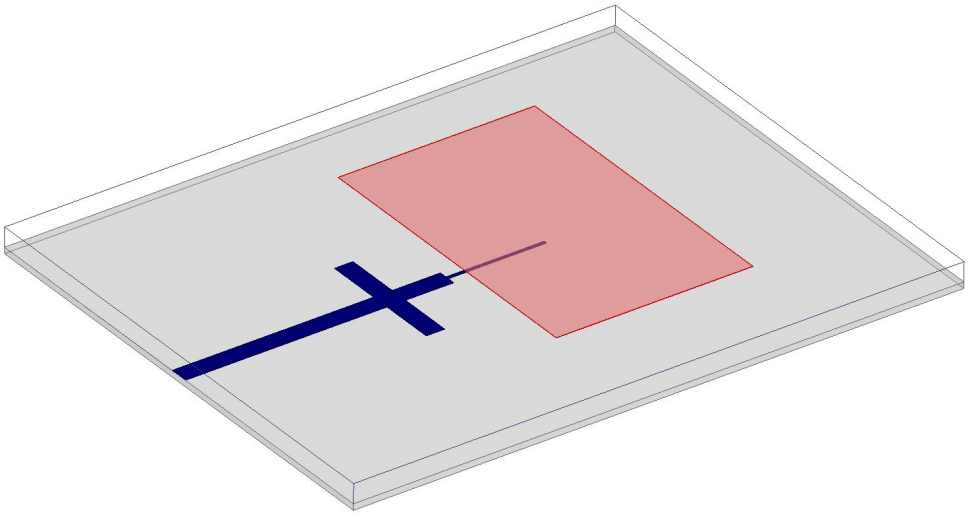

Figure 3.5: EM-coupled patch antenna (EMCPA) model

3.2.1 Radiating Element

The design of the radiating element follows a simple set of rules based on the design of an edge-fed patch antenna. First, the stack-up is decided, then the initial patch length is estimated using the following formulas [8]:

$$L = 0.5\frac{\lambda}{\sqrt{\varepsilon_r}} - 2\Delta L \tag{3.2}$$

where ΔL is the fringing length given by

$$\Delta L = 0.412\frac{(\varepsilon_{reff}+0.3)(\frac{W}{t}+0.264)}{(\varepsilon_{reff}-0.258)(\frac{W}{t}+0.8)}t \tag{3.3}$$

and ε_{reff} is the effective dielectric constant given by

$$\varepsilon_{reff} = \frac{\varepsilon_r+1}{2} + \frac{\varepsilon_r-1}{2}(1+\frac{12t}{W})^{-0.5} \tag{3.4}$$

The transmission line (TL) width is also calculated by numerical methods available in software for the desired impedance, which is normally 50 Ω. If the width of the TL turns out to be too large or too narrow, then different TL impedance may be considered.

This layout is then entered and simulated computationally using the finite element method with the Ansoft HFSS 14.0 software. The simulated S_{11} value is used to make adjustments to the patch length to ensure it resonates at the desired frequency. The simulation also evaluates the impedance of the TL at the edge of the patch, which is used to estimate the size and location of a double open-ended stub for impedance matching [6].

Finally, the model is updated with the stub, and using built-in optimization in the software its size and location is further fine-tuned for best response.

Initially, a 10 mil thick microstrip substrate and a 31 mil thick upper layer were considered. However, the required bandwidth was barely achievable and variations as small as 0.4 mil in the patch and feed placement and sizes reduced the bandwidth below the required value. Since the simulation is expected to yield only approximate results, and since manufacturing errors may up to 2 mil, this result was not acceptable. It was then decided to scale the thickness of both substrates by a factor of two in an attempt to increase the resonating volume and thus the bandwidth. This approach yielded a 6.8% bandwidth (Figure 3.6). Furthermore, the bandwidth dropped to 5% with up to 4 mil errors in the copper layout, which is an increase of an order of magnitude in error tolerance over the thinner sample.

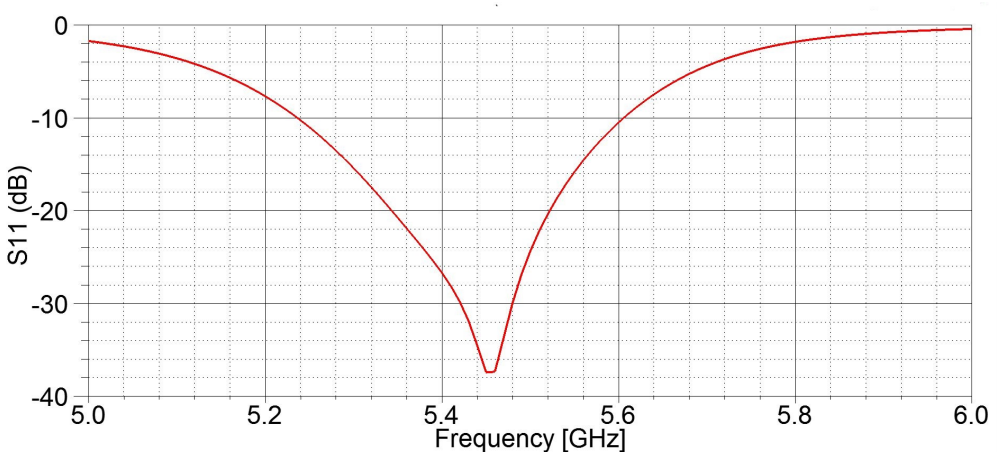

Figure 3.6: Simulated S_{11} response of the EMCPA

Table 3.3 summarizes the dimensions of the patch antenna and its simulated radiation characteristics.

Table 3.3: Radiating element dimensions for the EMCPA

Substrate material	Rogers RT/duroid 5880
Lower substrate thickness	20 mil
Upper substrate thickness	62 mil
Copper thickness	35 μm (1 oz.)
Patch length	16.1 mm
Patch width	25 mm
Coupling line width	0.25 mm
TL width / tuning stub width	1.5 mm
Tuning stub distance from patch (edge-to-edge)	4.7 mm
Tuning stub length (total)	10.5 mm
Simulated center frequency	5.42 GHz
Simulated -10 dB bandwidth	369 MHz (6.8%)

3.2.2 2-Dimensional Array

Having shown that sufficient bandwidth can be achieved with the EMCPA radiating element with a reasonably sized stack-up, the next step was to design a feeding network that would allow proper phasing and power tapering.

Since the feed line terminates under the patch, the feed network needed to route power to each patch from a central main feed. This meant there would be several junctions in the feed network regardless whether the design was corporate or series-fed. Therefore, in order to minimize the distance from the source to the farthest cell the connection to the antenna was placed at the center of the panel. As such, four quadrants needed to be connected in parallel. The 8 patch antennas in each quadrant were decided to be connected in series, since parallel feeding would have made the antenna substantially wider. With these constraints in mind, a general approach to the layout is illustrated in Figure 3.7.

The increased path length between unit cells was to ensure that the electrical length between them remained one wavelength in order to ensure the branches are in phase. Also, since mutual

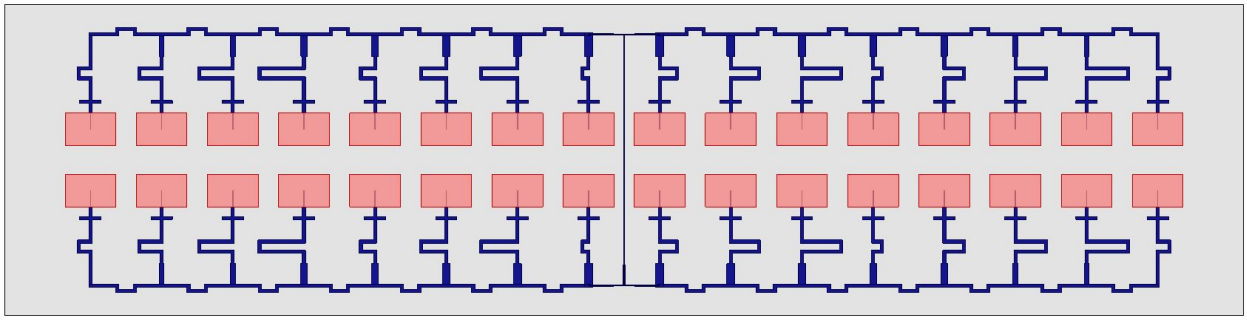

Figure 3.7: 2 x 16 phased array antenna layout using EMCPA

coupling in the feeding network path extensions was to be avoided, it would have added significant width to the antenna.

There are several problems with this layout, besides its width. First, it contains lots of different quarter-wave transformers, T-junctions and length extensions; therefore, its feeding network is very inefficient in terms of increased power loss and physical size. Second, the electrical length between adjacent patches is at least three times the wavelength. The effect of this is that the beam direction will change considerably with frequency change. In the beam-steer equation (Equation 3.1), the phase difference between adjacent elements connected by a TL of total length L is given by

$$\Delta\phi = \frac{L \bmod \lambda}{\lambda} \times 360^{\circ} \tag{3.5}$$

Substituting the values from Table 3.2 into Equations 3.1 and 3.5, and assuming $L > 3\lambda$ and $F = 5.43\ GHz$ yields $L = 0.12\,m$. (Note the speed of light in copper is about $0.66c$, lowering the wavelength to about 2/3 of that in vacuum.) If this value is now used to calculate the resulting beam direction for $F = 5.33\ GHz$ (the lower end of the required bandwidth), the result is $\Theta = 20^{\circ}$. This amounts to a 5° change in beam direction, which is highly undesirable. To continue with this design, other mechanisms would have to be included to ensure the electrical length of the TL between adjacent patches remains unchanged with frequency.

The EMCPA approach has thus yielded a complicated design with several unanticipated obstacles and drawbacks. At this point, the attention was directed towards a different kind of patch architecture, which eventually proved to be the better choice.

3.3 Aperture-Coupled Patch Antenna Array

Aperture-couple patch antennas (ACPA) offer yet another different approach to excite the patch indirectly through electromagnetic coupling. The feed and the patch layers are on different planes similarly as in an EMCPA, but in this case the microstrip is inverted, i.e. the ground plane is between the feed and the patch. To allow the signal to couple to the patch, a hole is cut in the ground plane hence the name. The model of an ACPA is show in Figure 3.8, where the slot length is exaggerated for illustration purposes.

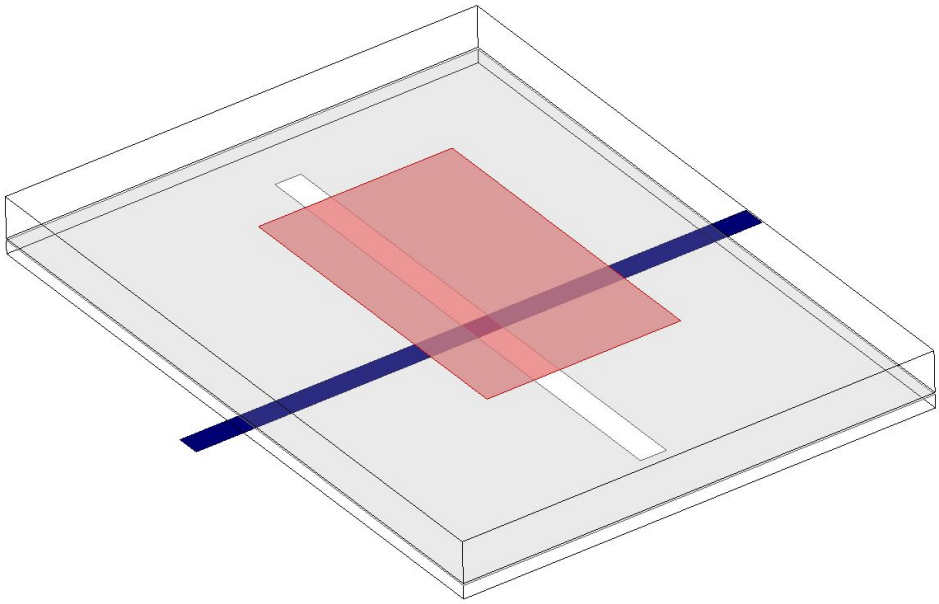

Figure 3.8: Aperture-coupled patch antenna (ACPA) model

The ACPA has more design variables than the EMCPA which can be tuned to achieve the desired radiating characteristics. This makes ACPAs more versatile to design against competing requirements. As explained in the previous section, the power delivered to the EMCPA could only be varied by adjusting the impedance of the feed to the individual patch. In the case of the ACPA,

the feed can be kept constant, and the coupling power adjusted by varying the slot size and position. In addition, since the feed line passes through under the patch, this arrangement lends itself to a much simpler series feeding network.

On the other hand, the search-space is increased and the computations become more complex, which causes a more iterative design procedure. The stack-up and the radiating element need to be more carefully considered to ensure that later requirements will be met.

3.3.1 Stack-up

It has already been discussed that the exposed feed line on the bottom of the ACPA is not desired, and with this design a stripline architecture is to be used to ensure that the back side of the antenna is grounded. For the same dielectric height and impedance, the stripline width is about 1/2 the microstrip. A too thin feed line carries the risk of not being able to handle the current flowing through it. Later in the design it will be shown that a power divider needs to be used, which has sections requiring a 100 Ω impedance. A 40 mil thick symmetric stripline with a width of 0.88 mm has characteristic impedance of 50 Ω, while the 100 Ω line is 0.22 mm wide. This is close to the lower limit for the width of a 1/2 oz. copper TL carrying 1 W. Therefore, the stripline cannot be thinner than 40 mil.

With this in mind, the ACPA was modeled with the Ansoft Designer 8.0 software. Initially, a 31 mil thick upper subtrate was used with the 40 mil stripline, but later it was found that the gain of the antenna array was not satisfactory. Instead a 62 mil upper substrate was used, which yielded adequate results. The adhesive, as discussed in section 3.1.3, was also added to the simulation. The complete layer-by-layer stack-up of the ACPA is shown in Table 3.4 and Figure 3.9.

3.3.2 Radiating Element

The design of the radiating element is similar to that of the EMCPA. The initial patch length is estimated using equations 3.2, 3.3 and 3.4. The reasons for the patch width are the same as with the other design, and so it is fixed at 25 mm. The slot opening is placed at the center of the patch.

Table 3.4: Complete stack-up of the final ACPA design

Layer	Material	Thickness
Cover	Duroid 5880	10 mil
Adhesive	Rogers 2929	3 mil
Patches	copper	0.5 oz
PCB	Duroid 5880	62 mil
Adhesive	Rogers 2929	3 mil
GND with slots	copper	0.5 oz
PCB	Duroid 5880	20 mil
TL	copper	0.5 oz
Adhesive	Rogers 2929	3 mil
PCB	Duroid 5880	20 mil
GND	copper	0.5 oz

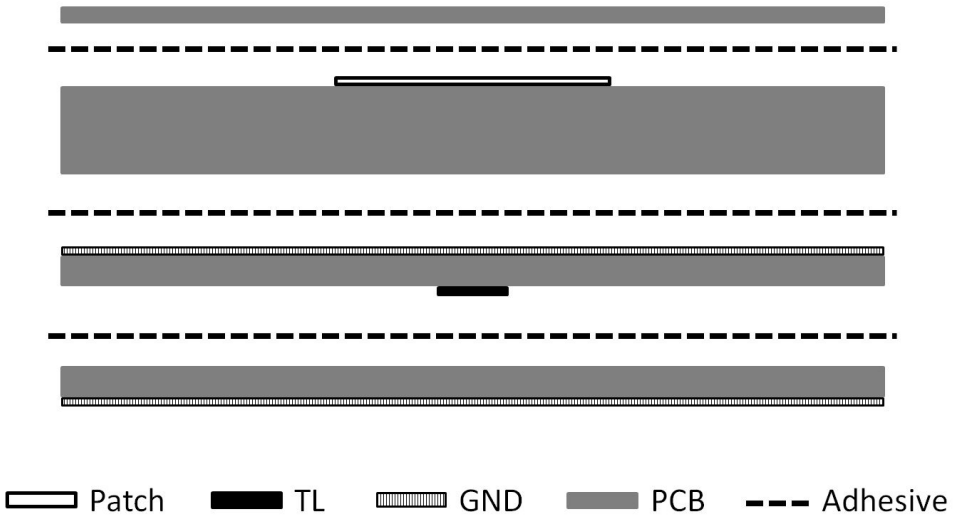

Figure 3.9: Complete stack-up of the final ACPA design

As for the size, several factors are to be considered. First, the width of the slot should not be more than about 1/10th of the length. The length of the slot affects the center radiating frequency, the power coupled to the patch and the impedance of the patch. The slot should not reach beyond the edges of the patch, but it needs to be large enough to allow coupling. With these in mind, the slot size was set to be 1 mm wide to allow the length to be varied between 10 and 25 mm.

Since the slot length also influences the resonant frequency of the patch, it does not make sense to characterize the bandwidth of an individual radiating element. Instead, the bandwidth will be assessed when the power-tapered array is simulated.

3.3.3 *Linear Array*

Extending the ACPA radiating element into a linear array is fairly easy; the feed line is a simple serpentine line placed under the patches (Figure 3.10). The length of the feed between adjacent slots determines the phase shift. First, a 2-port array with a 50 Ω input and a terminated resistive 50 Ω end is simulated with identical middle elements. This is to ensure that the non-tapered and ideally terminated array gives beam characteristics comparable to the calculated case.

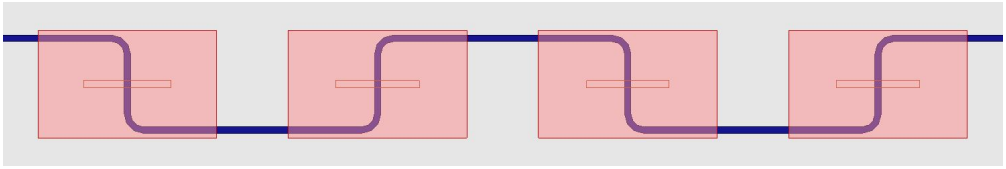

Figure 3.10: Layout of a series-fed ACPA array

For this case, the 15-element array is simulated first in an attempt to keep the length of the antenna under 22" for cost savings (section 3.1.2). Also, since the array is series-fed, the number of elements does not make a difference in the design of the layout. The biggest impact of the size reduction is the increase of beam width, the amount of which may or may not necessitate the use of the larger size.

The antenna was fine-tuned by adjusting the feed length between the adjacent elements to achieve the desired 25° beam direction. Figure 3.11 shows the simulated radiation pattern, which agrees quite well with Figure 3.3 confirming the validity of the design. However, as expected, the beam width increased from 5° to 7°. After consideration, this was decided to be an acceptable compromise to keep manufacturing costs down.

3.3.4 *Power Tapering*

The expected maximum side lobe level of a uniformly excited linear array is -12 dB, which is confirmed by the simulated pattern shown in Figure 3.3. In order to bring it further down, a 15-element -20 dB Taylor power taper needs to be applied to the patches. The normalized power levels are shown in Table 3.5.

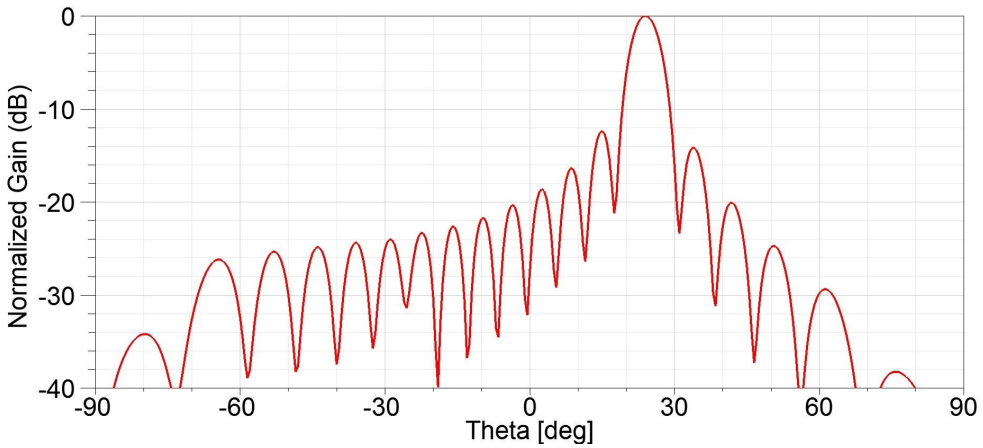

Figure 3.11: Simulated radiation pattern of the 2-port ACPA array

The power delivered to the patches down the serpentine TL is varied by the slot length of each patch. In order to calculate what slot length each patch needs to have to radiate the exact power required by the tapering, a synthesis method described by J. Salazar et al in [17] was employed. In this approach, the array of patch antennas are replaced by an equivalent circuit comprised of TL segments connected in series with load impedances between them. The last patch antenna of the array is a 1-port load, whereas the middle antennas are 2-port. Figure 3.12 shows the equivalent circuit of the linear array antenna, with Z, P, and Γ representing impedance, power and reflection coefficient, respectively. "-" indicates the incoming values, and "+" indicates the outgoing values of the antenna section.

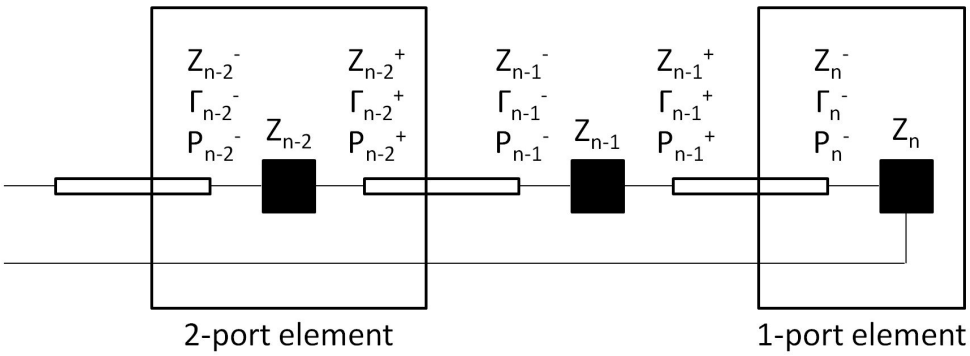

Figure 3.12: Equivalent circuit of the series-fed linear array antenna

Table 3.5: 15-element -20 dB Taylor power taper values

Element #	Relative Power
1	0.593
2	0.597
3	0.636
4	0.729
5	0.847
6	0.941
7	0.988
8	1.000
9	0.988
10	0.941
11	0.847
12	0.729
13	0.636
14	0.597
15	0.593

In this circuit, the following equations describe the relationships between power and impedance [17]:

$$\Gamma_n^- := \frac{Z_n^- - Z_0}{Z_n^- + Z_0}\,, \quad n = 1,\ 2,\ ...,\ N \tag{3.6}$$

$$M_n := \frac{S_{12}S_{21}\Gamma_n^-}{1 - S_{22}\Gamma_n^-}, \quad n = 1,\ 2,\ ...,\ N \tag{3.7}$$

$$Z_{n-1}^- = -Z_0\frac{S_{11} + M_n + 1}{S_{11} + M_n - 1}\,, \quad n = 1,\ 2,\ ...,\ N \tag{3.8}$$

$$P_{n-1}^+ = P_n^- \frac{\left(1 - |\Gamma_{n-1}^+|^2\right)|1 - S_{22}\Gamma_n^-|^2}{|S_{21}|^2|1 - \Gamma_n^-|^2}\,, \quad n = 1,\ 2,\ ...,\ N \tag{3.9}$$

$$Z_{n-1} = \frac{Z_{n-1}^+ P_{n-1}}{P_{n-1}^+}\,, \quad n = 1,\ 2,\ ...,\ N \tag{3.10}$$

For a known impedance of the last element (Z_N), TL S parameters, and required power ratios, equations 3.8, 3.9 and 3.10 allow to calculate the impedances of the middle elements iteratively from the last to the first. The key to this design is to find a patch size and slot width (or slot shape if the simple rectangular slot is not appropriate), which allows the patch to be tuned for the required impedance by adjusting the slot length alone. The impedance of the last element also influences what range of impedances the middle elements will have; therefore, the next steps of designing the 1-port end element and the 2-port middle elements is an iterative process which are repeated until an acceptable solution is achieved.

3.3.5 1-port End Element

The linear array discussed before was terminated by a simulated 50 Ω resistor. For simplicity, an actual resistor in the physical antenna was initially considered. There are a different ways to achieve that. First, an embedded resistor can be used in the PCB. However, bending the board may cause the resistor to get displaced or weaken the connection. Also, the manufacturer ultimately chosen for building the antenna would not be able to add embedded elements. Second, a resistive layer could also be added to the stack-up. Lastly, routing the end of the TL to the edge of the board and adding a connector would allow to attach an external resistor. These last two options were discarded in part for the increased complexity of manufacturing. More importantly, the resistor would lower the efficiency of the antenna, and so this idea was also ultimately discarded.

With these considerations it was decided that an open-ended serpentine line would be used. The problem with that is that the reflected wave from the open end travels down the array backwards with the same phase-difference as the forward signal thereby creating a substantial sidelobe at the -25° direction (Figure 3.13).

In order to eliminate the reflected signal, the last element of the array needed to be tuned for 50 Ω impedance using simple stub tuning. For this, a suitable slot length and final TL length had to be selected, which allows convenient placement of the stub at a straight section of the feed line as well as limits the power radiated by the stab. This is needed since the array would be power-

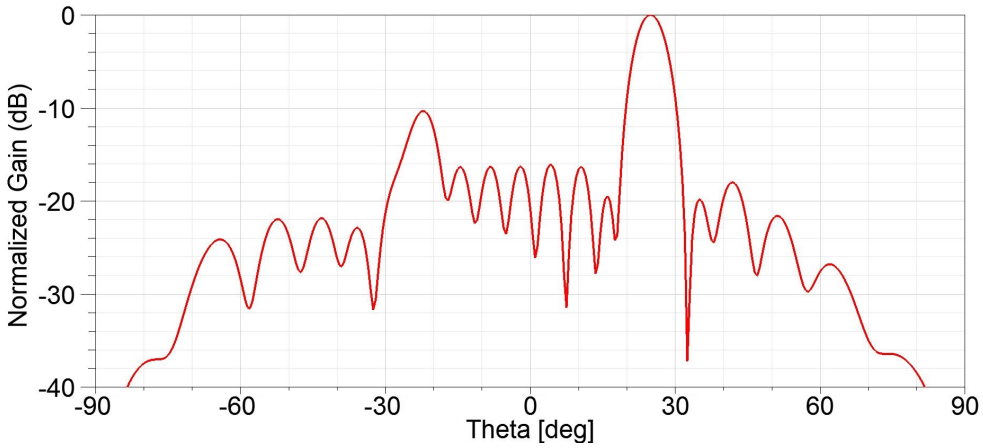

Figure 3.13: Simulated radiation pattern of the open-ended 1-port ACPA array showing the side lobe introduced by the reflected signal

tapered, meaning that the end element would need to get a small amount of power in comparison to the middle elements. The slot was selected to be at the shorter end of the resonant curve and adjusted in length to allow for a convenient stub size and location. The dimensions of the finalized end element is shown in Table 3.6, and its layout in Figure 3.14.

Table 3.6: End element dimensions for the ACPA array

Patch length	15 mm
Patch width	25 mm
Slot length	6.5 mm
Slot width	1.0 mm
End TL length (from slot)	7.8 mm
Stub distance (from slot)	1.2 mm
Stub length	7.2 mm

3.3.6 2-port Middle Elements

When designing the 2-port elements, the primary objective is to ensure that the slot length variation can provide the range of patch impedances which are required for power tapering. With the synthesis method described in Section 3.3.4, and the simulated impedance of the end element, the

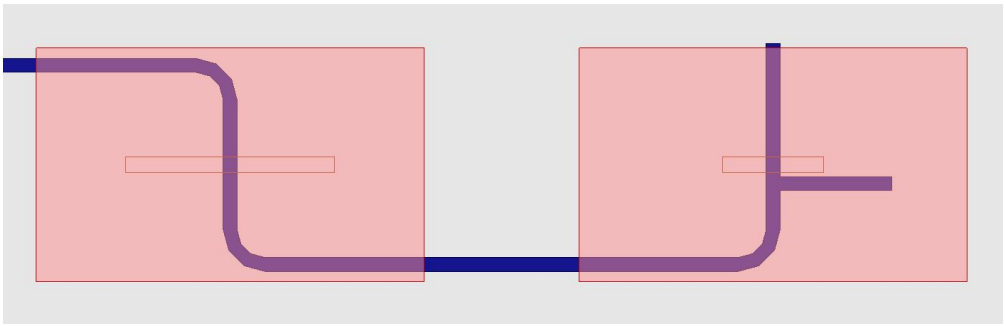

Figure 3.14: The last two elements in the ACPA array

range of impedances for the middle elements can be calculated. For the end element in the previous section, this range turned out to span from about 0.75 Ω to 13 Ω. With a patch size fixed at L = 15 mm and W = 25 mm, these impedances could be achieved by varying the slot lengths from 11 mm to 22 mm.

The impedance was simulated for the different slot lengths at 0.5 mm increments, and a best fit curves to the real and imaginary parts were determined by MATLAB software. In the synthesis method, when the impedance of the next element of the array was calculated, the curve was used to estimate the slot length that would result in the correct real part of the impedance. The complex impedance was then updated with the actual impedance of the selected slot length. These are summarized in Table 3.7, below.

Figure 3.15 shows the 1-dimensional array adjusted for insertion phases of the slots as well as with the tuned end element. Note the sharp decrease in gain at -25° verifying that the stub tuning eliminates the reflected wave from the open end.

3.3.7 2-Dimensional Array

Extending the series-fed 1-dimensional array is simple in this case, as the elevation beam direction is 0°. This means that no phase difference between the rows of patches needs to be introduced and they can be driven in parallel from a single input located somewhere on or close to the side of the antenna. The distance between the rows of patches, which drives the elevation beam width, has already been calculated. The simulation was updated with two rows in order to verify the validity

Table 3.7: Slot lengths of the middle elements for the ACPA array

Element #	Slot Length (mm)
1	22.0
2	21.3
3	20.1
4	17.9
5	15.6
6	14.0
7	13.1
8	12.2
9	11.7
10	11.5
11	11.7
12	12.4
13	13.1
14	13.5

of the calculations. Since no adjustments were necessary, the final step in the circuit-design was to add a power divider that distributes the signal evenly in phase between the two rows. The input and two outputs of the power divider are all 50 Ω. A simple symmetric T-junction can be used, but since the output impedances are halved, quarter-wave transformers were added to ensure proper impedance-matching. The layout is shown in Figure 3.16.

There are several methods to improve the efficiency and reduce the reflection of a T-junction [21]. However, all of those include making the output lines at the junction thinner, which may become unable to handle the power passing through them. The 100 Ω branches have a thickness of 0.22 mm, which is already close to the lower limit of a 1/2 oz. copper transmission line at 1 W power. The simulation showed satisfactory S-parameters for the illustrated circuit.

The model was then finally updated with the power-divider (Figure 3.17), and the simulation was run using a single input to evaluate the expected antenna characteristics.

At the center frequency, the H-plane radiation pattern (Figure 3.18) was the same as for the 1-dimensional array, and the E-plane radiation pattern showed a beam width of 50°, as expected.

Then, the simulation was run at the low and high ends of frequency ranges of the two radars, i.e. at 5.33 GHz, 5.41 GHz, 5.45 GHz and 5.53 GHz. The resulting radiation patterns are illustrated

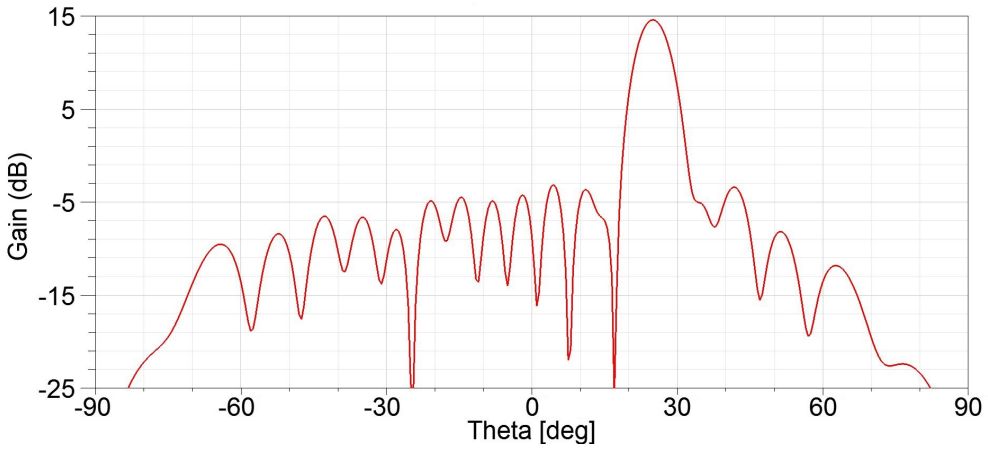

Figure 3.15: Simulated radiation pattern of the 1-dimensional array at the center frequency (5.43 GHz)

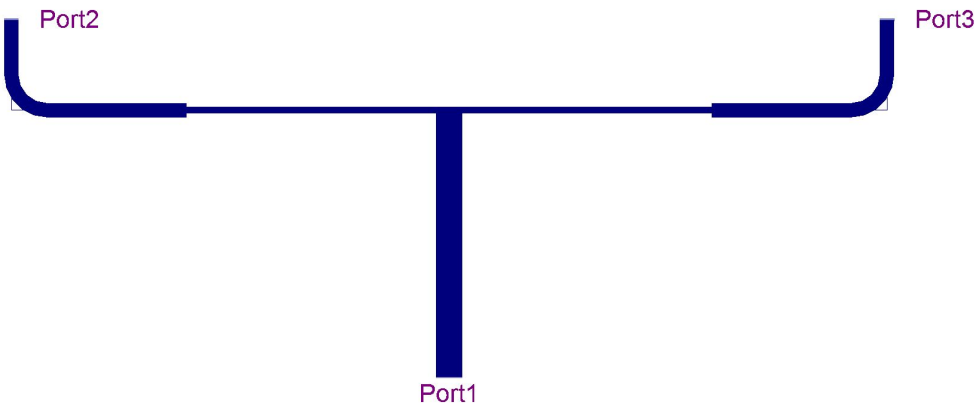

Figure 3.16: Layout of the power divider

in Figure 3.19. The beam direction changed by up to 3° away from the desired direction, and the beam width also varied from 5° to 8° as the frequency increased. This was decided to be acceptable for this design. Also, the maximum side lobe levels increased as the frequency was changed further from the center frequency. With slight adjustments of the TL line length between the patches with additional software optimization, it was possible to keep the side lobes below -15 dB across the required bandwidth. On of the reasons for the increased side lobe is the fact the last element is tuned for the center frequency, which allows more reflections in the extreme ends of the bandwidth.

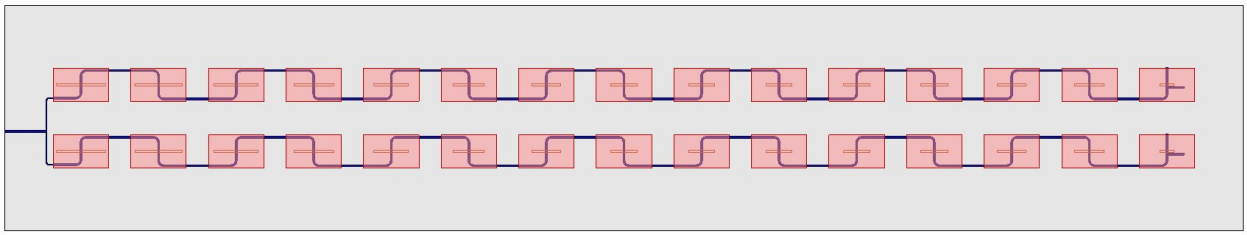

Figure 3.17: Layout of the final design

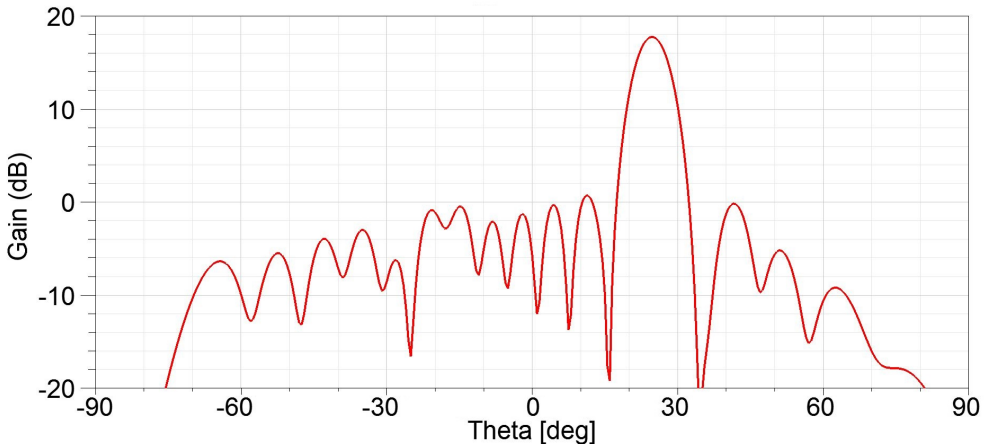

Figure 3.18: Simulated radiation pattern of the final design at the center frequency (5.43 GHz)

The simulated S_{11} response of the antenna is shown in Figure 3.20. Within the operating frequency range of 5.33 - 5.53 GHz, S_{11} is well below -10 dB.

3.3.8 Connector

The required connection to the radar system is through a standard 50 Ω SMA connector. The feed line at the antenna input was designed to be 50 Ω so that no additional impedance matching is necessary. The stripline architecture is unbalanced just like the coaxial cable; therefore, no balun or additional hardware is needed as longs as the signal is connected to the feed line and the ground to the two ground planes. The connection is usually made via soldering or pressure contact, which means that the feed line and the middle ground plane both need to be physically accessible. This can be achieved by cutting out pieces from the different PCB layers at precise locations to expose the required amount of copper which would otherwise be hidden inside the antenna.

Another way of accessing the hidden copper would be to add vias inside the boards to route

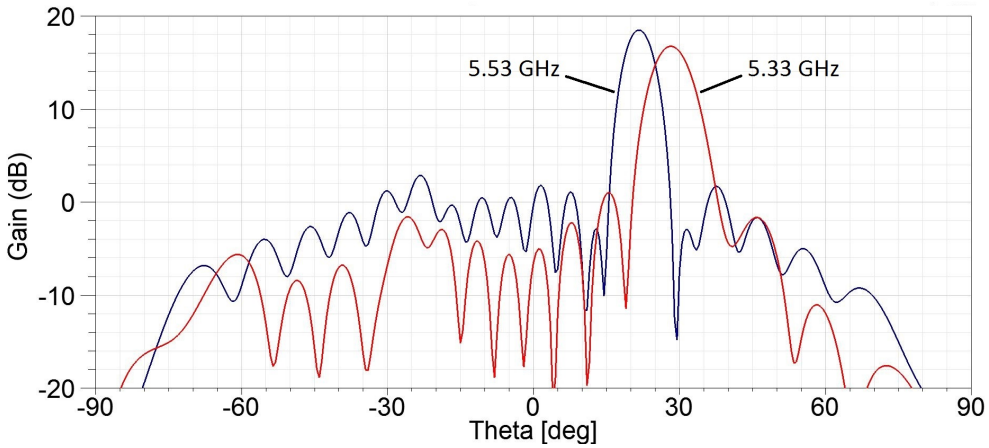

Figure 3.19: Simulated radiation pattern of the final design across the required bandwidth (5.33 GHz - 5.53 GHz)

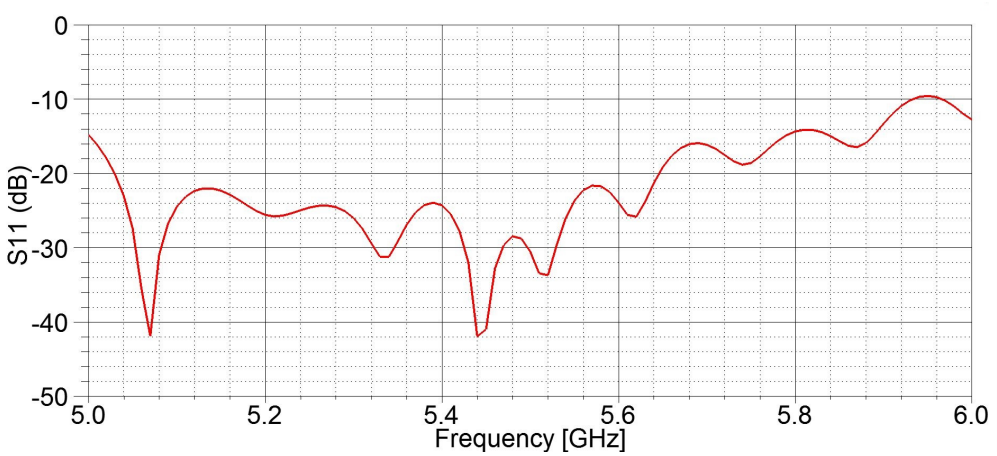

Figure 3.20: Simulated S_{11} response of the final design

metallic connection from the outside to them. However, this is not desired for the same reasons as why probe-fed antennas were not considered; i.e. cost of manufacture and flexibility of the boards.

Furthermore, the edge cut-outs allow a side-mounted connection as opposed to a surface mount if vias are used. The former is better suited for our case, as it allows the cable to be run parallel to the aircraft fuselage and gives flexibility as to the routing of the cable to the inside of the plane. (A back-mounted connector may need a matching hole in the fuselage in the exact position where the antenna is if running the cable between the two is to be avoided.)

The amount of cutout depends on how and what kind of connector is going to be attached to the PCB. Simple SMA-connectors are usually made for a microstrip architecture, and standard

stripline SMA-connectors were not available for the PCB thicknesses that the antenna was designed with. In addition, the available stripline connectors were quite wide at 0.5”, which might have introduced problems when then antenna was to be bent. Because of these, it was decided that an SMA connector would be connected to a short rigid or semi-rigid coaxial cable, which in turn would be soldered directly to antenna. A computer-aided design (CAD) drawing of the top and bottom view of the board at the connector with the exposed copper is shown in Figure 3.21.

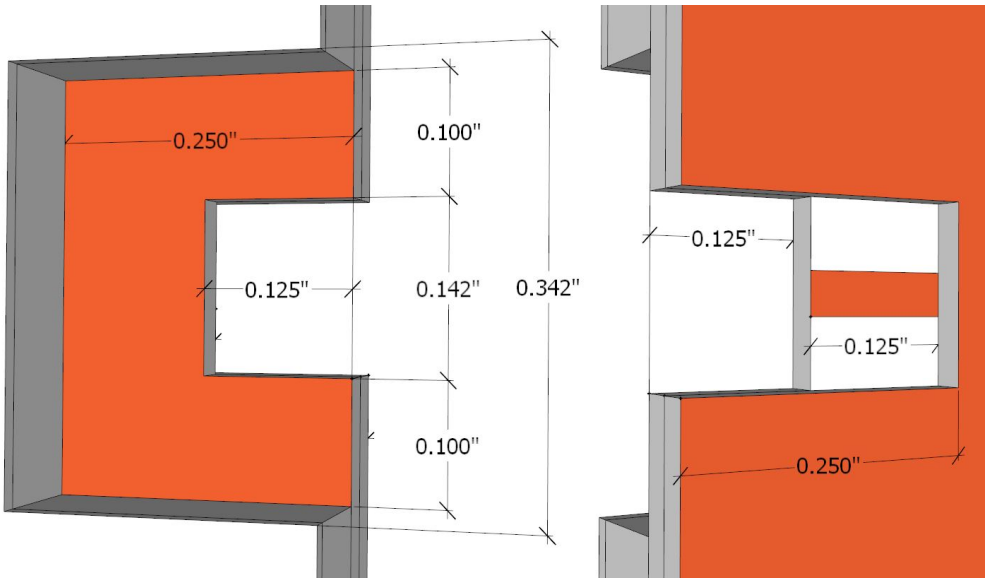

Figure 3.21: Top and bottom views of the antenna connection

3.4 Effects of Manufacturing Errors

Manufacturing errors may result in different antenna characteristics than those simulated with absolute precision. In order to estimate the extent of deviation from the designed radiation pattern, the effect of these errors were considered and simulated.

3.4.1 Trace Width

The etching process which creates the copper traces on the PCB has a precision of 2 mil, which is about 0.05 mm. The patch sizes and slot lengths were designed with a 0.1 mm precision, whereas the TL widths were specified to within 0.01 mm. Also, the patch and slot dimensions are on the

order of 10 mm, whereas the traces are less than 1 mm. The manufacturing error; therefore, will affect the antenna characteristics via the TL width deviation more substantially than the size error of the patches and slots. This is shown in Figure 3.22. In the extreme case, the beam direction was shifted by 0.8° , and side lobes increased by up to 1 dB.

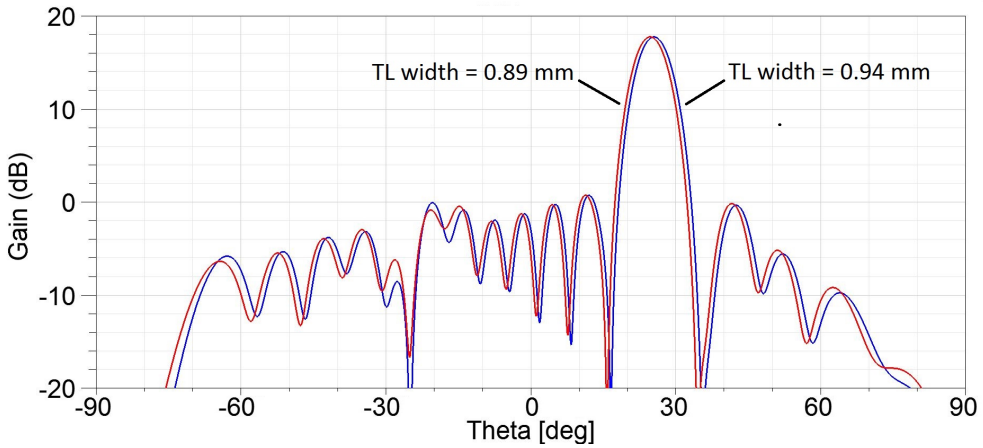

Figure 3.22: Effect of manufacturing error of the TL width

3.4.2 Stackup Layer Thickness

Anther source of error may be the thickness of the dielectric layers that compose the stack. In addition to the PCBs, these include the adhesive material between them. While the PCB thickness is expected to have low variance, the adhesive between them may vary by up to 1 mil, or 33% of the 3 mil design thickness. Figure 3.23 shows the resulting radiation pattern for that amount of error. In this case, the beam direction changed by 0.9°, with side lobes increasing by 2 dB.

3.4.3 Dielectric Constant

The dielectric constant of the PCB is given by the manufacturer as 2.20 ± 0.02, an error of 1%. The change of the radiation pattern with this amount of deviation was similar to those discussed before. The net effect in the beam pattern was slightly less, with a beam direction shift of 0.5° and a side lobe level increase below 1 dB.

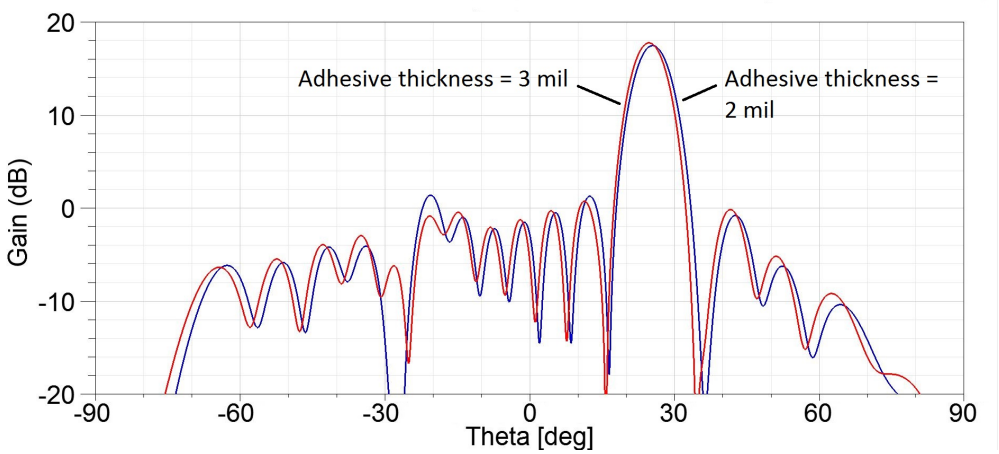

Figure 3.23: Effect of manufacturing error of the adhesive thickness

3.4.4 Layer Alignment

The relative positioning between the feed line, the slots and the patches can also affect the radiation characteristics. These three trace layers are etched onto two PCBs, with one PCB machined double-sided, and the other one single-sided. Whether the feed and slot traces or the slot and patch traces should be etched onto the same PCB was determined by considering which misalignment would cause a greater error in the resulting radiation pattern. The double-sided etching is inherently more precise than the lamination process; therefore, the traces that need to be more precisely aligned should be on the double-sided PCB.

The location of the slots with respect to the feed line determine the phase at which the patch will be excited, and if these are misaligned, the phase difference between adjacent elements will be non-uniform. Hence, the slot and feed traces were decided to be put on the double-sided PCB. The effect of misaligning the patches was then simulated. The finding was that a combined horizontal and vertical displacement of 0.5 mm (in each direction) contributed to almost no change in the radiation pattern.

Chapter 4. Experimental Results

As it was shown at the end of the previous chapter, a substantial source of manufacturing error is the thickness of the adhesive layers. For this reason, it was decided to have the antennas manufactured by a company which can not only create the individual PCB layers, but would also assemble the entire design.

Four manufacturers were contacted with a request for quote. Prototron Circuits and Out of the Box Manufacturing elected not to bid. Cirexx International quoted 7000 USD per unit for up to three boards. Hughes Circuits quoted 4000 USD for two antennas total. Reviewing these bids, Hughes was selected as the preferred vendor.

4.1 Fabrication Process

Originally, 1/2 oz. copper was to be used throughout, but due to shortages of the source material and in order to save the time required to backorder, 1 oz. copper was used instead. While not affecting the overall design and being better suited for the 100 Ω section of the power divider in the feed line, the thicker copper does increase the rigidity of the board substantially. However, it was estimated that the required curvature of the board would still be achievable.

Two antennas were ordered since the total quote remained the same for one or two units. Furthermore, having two antennas would allow to test both and compare them against manufacturing variations. Lastly, with two antennas SAR images could be taken by flying them on the aircraft as final verification and proof of concept.

Figure 4.1 shows the two antennas as received from the manufacturer.

Figure 4.1: The fabricated antennas as received from the manufacturer

4.1.1 Connector Attachment

The assembly was completed with the soldering of two coaxial cables with SMA connectors onto the two antennas. The ground of the coax was soldered to both ground planes in the antenna, and the signal soldered to the exposed signal line. A rigid and semi-rigid cable of varying length was used to assess the connection against mechanical forces. The antennas with the connectors attached are shown in Figure 4.2.

4.1.2 Panel Bending

Bending the panel was only attempted after the flat panel measurements were completed. Lengthwise the antennas proved to be easily bendable. However, this design called for crosswise bending, which turned out to be not feasible by hand. The lamination process created extra stiffness in the board, which necessitated mechanical bending. First, an edge press was used for bending, but due to the availability of only low-diameter die (less than 1”), it was only possible to bend the board at quarter-inch increments adding a lot of sheer at the pressure points which could be seen on the surface of the board (left antenna on Figure 4.3). This antenna had a curvature radius of 0.18 m. Due to the previous fracture of this board at the connector, no measurements could be made to

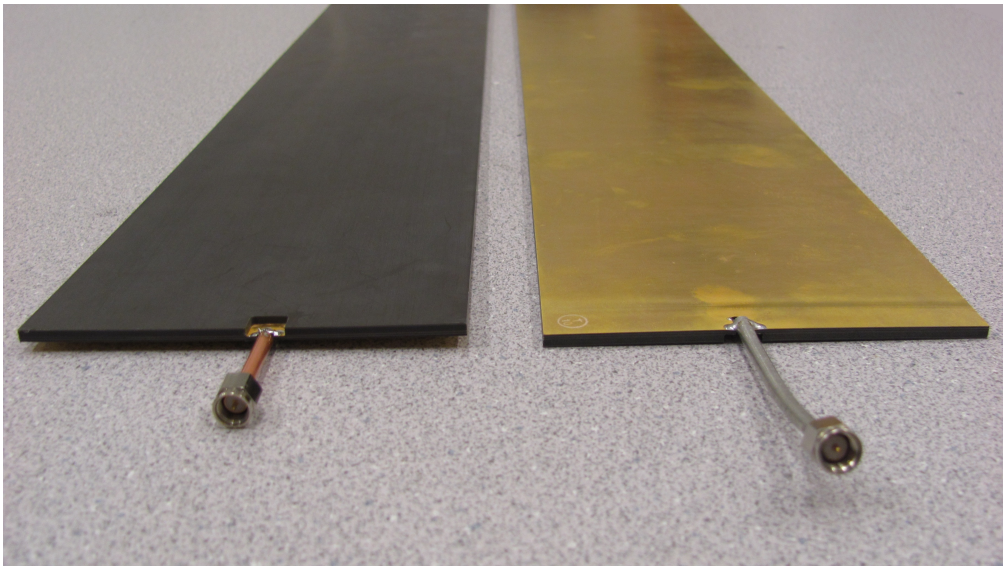

Figure 4.2: The antennas with the connectors attached

check the effects of this type of bending. The second board was then bent using a different edge press with a 3.5" die and added lubricant to protect the surface from friction forces. With this method, a 0.25 m radius permanent curvature was achieved, and the antenna characteristics were subsequently measured.

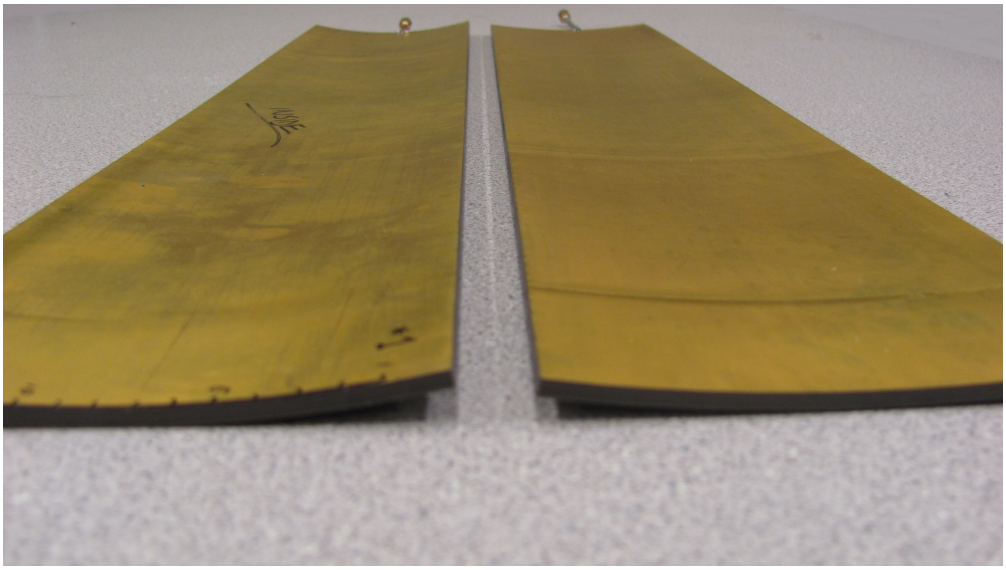

Figure 4.3: The antennas after bending

4.2 Antenna Measurements

The antennas were tested to verify whether the design goals have been achieved. The return loss was first checked as a general test to check for obvious defects. Then, the radiation patterns in the H-plane and the plane defined by the main lobe direction for both co- and cross-polarized were measured. Using a calibrated standard gain horn antenna, the gain was also calculated. This was repeated for the flat antenna as well as the curved antenna.

4.2.1 Return Loss

The return loss, or voltage standing wave ratio, was measured by directly connecting the antennas to a network analyzer (NWA). After a 1-port S_{11} calibration of the NWA, the return loss was measured between 5 GHz and 6 GHz. The resulting plot is shown on Figure 4.4 for one of the antennas. Both antennas yielded a similar S_{11}. In the design frequency range between 5.33 GHz and 5.53 GHz, both antennas were measured as having peak return losses below -13 dB. In addition, the bandwidth of the antennas as defined by the below -10 dB return loss criteria is more than twice as much as the required bandwidth. After bending the antenna, the return loss measurement was repeated. It yielded a very similar result to that of the flat antenna, suggesting that the circuitry was not damaged by the bending process.

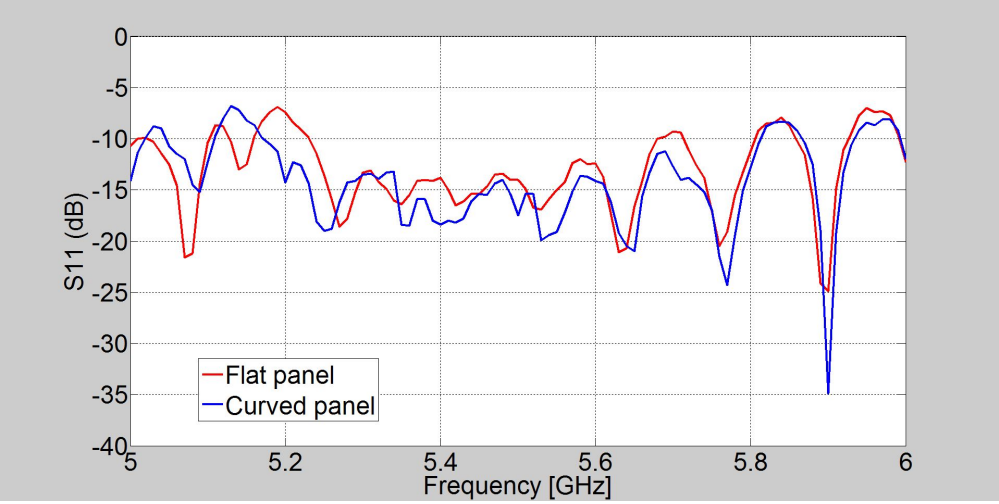

Figure 4.4: Measured S_{11} of one antenna

While this result is substantially different from the simulated return loss, it still meets the below -10 dB design requirement at the design frequency range to provide efficient radiation and adequate bandwidth. On the other hand, the return loss rises as the frequency is changed further away from the center, confirming that the circuit is indeed tuned for the right frequency. The inconsistency between simulated and measured return loss may be attributed to the soldering in the connectors and the transition from the coaxial signal to the feed line as well as manufacturing errors in the circuit.

4.2.2 Equipment Setup

The radiation pattern measurements were made using a NWA attached to a Vivaldi antenna as transmitter, and to the antenna under test (AUT) as receiver. In order to make measurements in the far-field, antennas had to be separated by at least the Fraunhofer distance, which is given by

$$r = \frac{2D^2}{\lambda} \tag{4.1}$$

where D is the largest physical length between radiating parts of the antenna, and λ is the wavelength. In this case, $D \approx 0.52\ m$, $\lambda \approx 0.055\ m$, giving a far-field range of about 10 m. On one hand, this distance and length of cables necessitates the use of an amplifiers. On the other hand, 10 m exceeds the length of the anechoic chamber of the Department of Electrical Engineering at the University of Washington. The compromise solution was to place the AUT in the chamber, and the Tx antenna outside of it at a sufficiently large distance. To keep the signal-to-noise ratio (SNR) low, two amplifiers were added to both the Tx antenna and the AUT. Using this arrangement, an SNR of more than 40 dB was obtained. The NWA was also connected to a computer which recorded the S_{21} transmission values and controlled a stepping motor which rotated the AUT horizontally at 1° increments between -90° and 90°. The schematic of the setup is illustrated in Figure 4.5.*

*Pictures of the test equipment are listed in Appendix B.

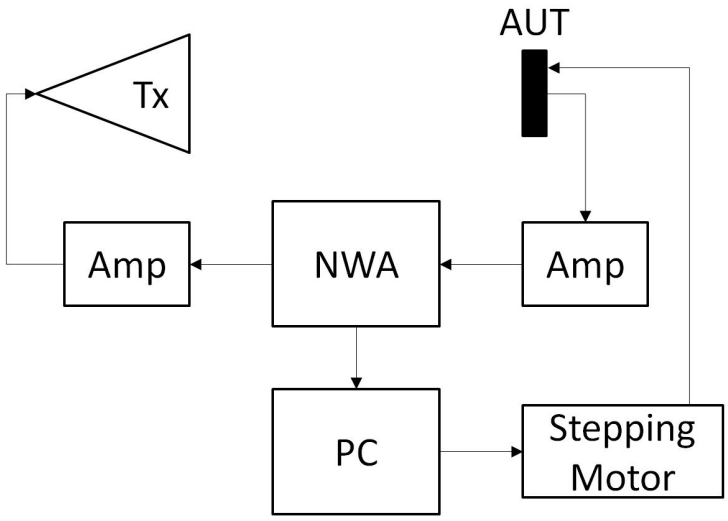

Figure 4.5: Experimental setup for radiation pattern measurement

4.2.3 Methodology

Radiation pattern measurements greatly depend on proper alignment and gain calibration. The Tx antenna needs to be at the same height as the AUT and directed horizontally towards the center of it. The AUT in turn also needs to be aligned to be facing the AUT at 0°. Calibration is achieved using a standard gain antenna, which in our case was a standard gain horn calibrated at 5.8 GHz.

For H-plane pattern measurements a total station was set up at the marked position of the front of the Tx antenna. The AUT was then set atop the rotating platform facing the station. Markers were added to the left and right sides of the AUT and the distance from the station was measured with 0.1 mm accuracy. The AUT was adjusted such that the left and right sides were equidistant from the total station ensuring the alignment was accurate to within 0.1°. This was repeated every time when the antenna was placed on the rotating platform. For beamf-plane measurements the horizontal alignment was made by rotating the AUT and Tx until maximum S_{21} gain was observed in the NWA. The Tx antenna was then aimed at the center of the AUT and vertically adjusted until maximum S_{21} gain was observed. A custom software written by John Mower at UW was then used to rotate the platform with the AUT and record angle and S_{21}. The process was repeated several times for H- and beam-plane co- and cross-polarization setups.

Each measurement was repeated at least 3 times to estimate the error which would come from

misalignment and interference. More emphasis was placed on determining antenna characteristics at the center and low and high ends of the bandwidth (5.33 GHz, 5.43 GHz, and 5.53 GHz), while measurements were also made at 5.41 GHz and 5.45 GHz for the bandwidth limits of the two radars.

4.2.4 Flat Panel

The radiation patterns of both antennas were measured, with a particular interest in determining azimuth and elevation beam direction and beam width, maximum side lobe level, peak gain, and differences between the two antennas to estimate manufacturing errors. Figures 4.6 and 4.7 show overlays between the simulated and the measured radiation patterns at the center frequency. (Additional figures with both co- and cross-polarization measurements and at other frequencies are listed in Appendix C.)

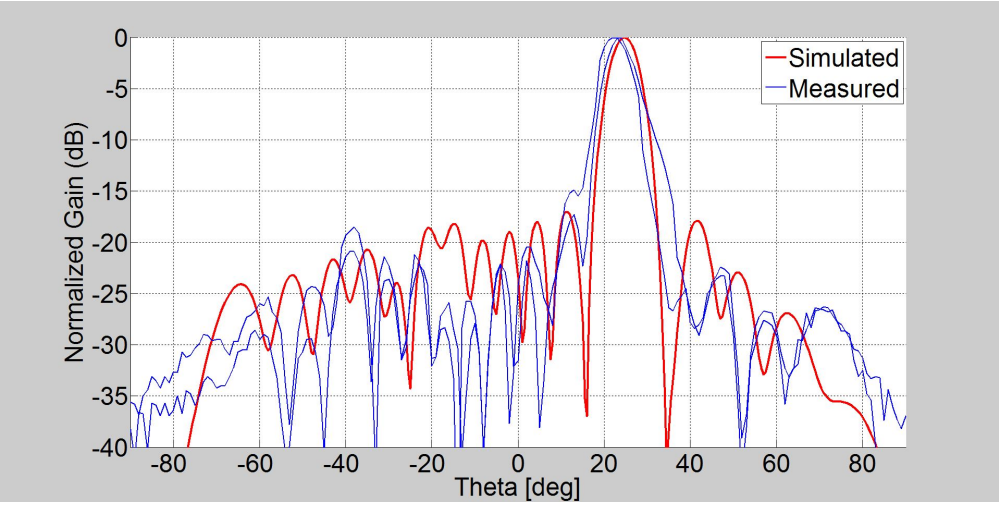

Figure 4.6: Simulated vs. measured H-plane radiation patterns at 5.43 GHz

From the figures it can be seen that the general direction and width of the main lobe follow the expected contour. Maximum side lobe levels are somewhat higher especially along the edges of the main lobes. Furthermore, the side levels seemed to vary by as much as 5 dB across different measurements. This could be attributed to reflections from the surroundings of the experimental setup. As mentioned before, a significant portion of the area where measurements were made was

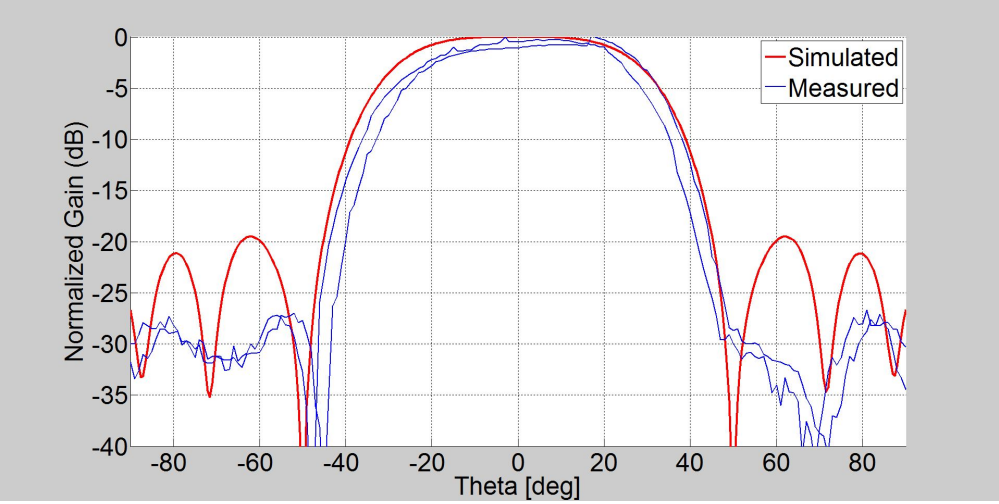

Figure 4.7: Simulated vs. measured beam-plane radiation patterns at 5.43 GHz

outside of a chamber with several reflective surfaces. The summary of the measured characteristics are listed in Table 4.1. The elevation beam plane measurements were made at a fixed 25° vertical inclination of the antenna. Since the horizontal main beam direction changed by up to 7° with the frequency, this introduced substantial distortion in the measured elevation beam pattern. The largest difference in horizontal beam angle and the angle at which the antenna was placed on the platform during the measurements was at 5.53 GHz. At this frequency, the measured elevation beam pattern was no longer indicative of the actual radiation pattern in the 20° horizontal beam direction. This is indicated with a * in the table below.

Table 4.1: Measured flat-panel antenna characteristics

	5.33 GHz	**5.41 GHz**	**5.43 GHz**	**5.45 GHz**	**5.53 GHz**
Gain (dBi)	16.7 ± 0.2	17.8 ± 0.2	17.6 ± 1.4	17.9 ± 0.3	19.1 ± 0.2
Main beam dir. (deg)	26.8 ± 0.3	25.1 ± 0.3	23.4 ± 0.6	23.4 ± 0.3	20.4 ± 0.3
Main beam width (deg)	8.9 ± 0.3	8.3 ± 0.5	7.8 ± 0.6	7.8 ± 0.7	7.0 ± 0.7
Rel. side lobe (dB)	-13.3 ± 0.3	-16.1 ± 0.9	-16.4 ± 1.3	-19.1 ± 0.6	-15.2 ± 1.3
Rel. x-pol gain (dB)	-28.4 ± 1.6	-26.5 ± 0.2	-24.9 ± 1.4	-25.2 ± 0.3	-22.9 ± 0.3
Elev. beam width (dB)	43.4 ± 0.9	47.0 ± 2.0	47.5 ± 2.5	55.7 ± 0.6	72.2* ± 3.6
Elev. rel. x-pol (dB)	-17.4 ± 0.7	-23.1 ± 0.6	-21.2 ± 1.0	-23.0 ± 0.8	-13.5* ± 1.9

4.2.5 *Conformal Panel*

After bending the antenna, the H-plane and beam-plane radiation pattern measurements were repeated. Figures 4.8 and 4.9 show the comparison between flat and curved panel measurements at the center frequency. (Additional figures for other frequencies are listed in Appendix C.)

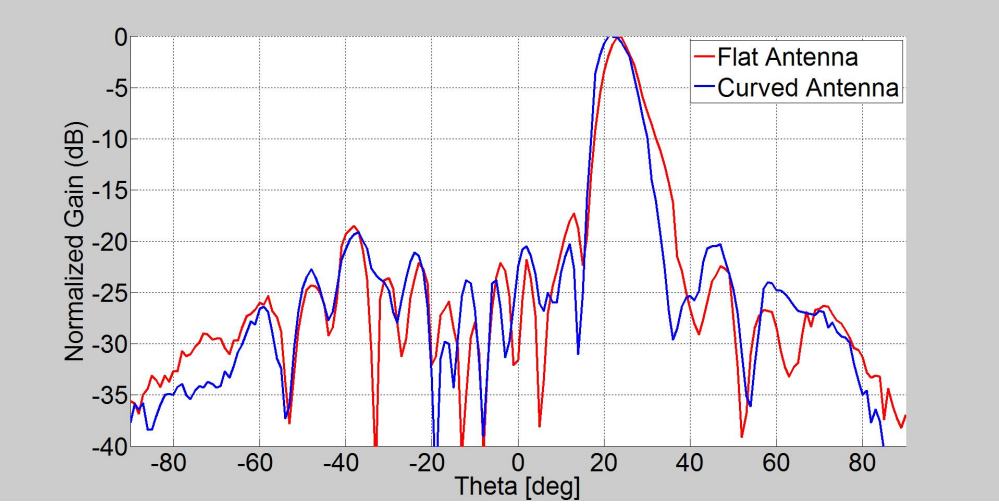

Figure 4.8: Flat vs. conformal antenna H-plane radiation patterns at 5.43 GHz

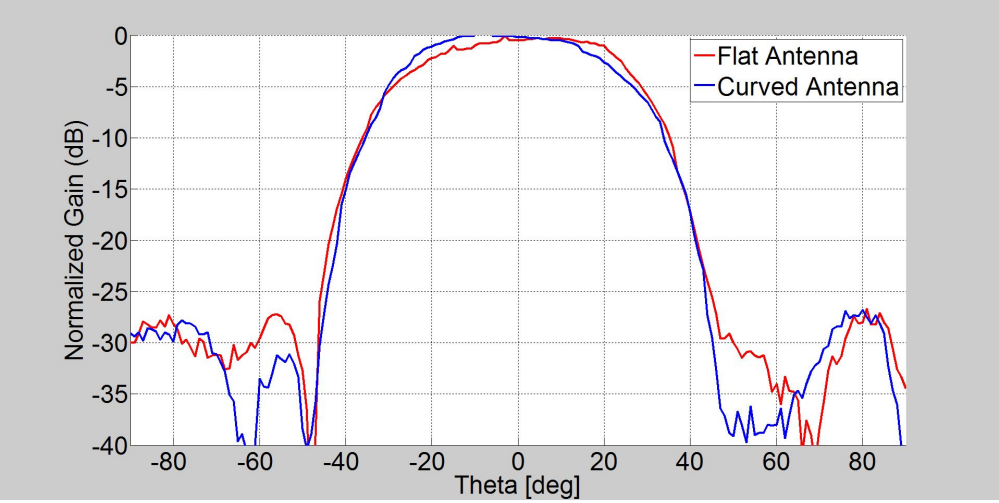

Figure 4.9: Flat vs. conformal antenna beam-plane radiation patterns at 5.43 GHz

As expected, neither the elevation nor the azimuth radiation patterns changed measurably. Main lobe direction, width, and side lobe levels stayed within the error of the measurement across the operating frequency ranges. The curvature and the bending process did not affect the radiation characteristics of the flat antenna, which are summarized in Table 4.2 below.

Table 4.2: Summary of measured conformal antenna characteristics

Mass	400 g $\pm$ 5 g		
Flat panel size (L x W x H)	56 cm x 10 cm x 0.3 cm		
Curvature radius	25 cm		
Bandwidth (S_{11})	440 MHz (8%)		
Elevation beam width	47°		
	@5.33 GHz	**@5.43 GHz**	**@5.53 GHz**
Gain	16.5 dBi	18 dBi	19.5 dBi
Beam direction	27°	23.5°	20°
Beam width	9°	8°	7°
Maximum side lobe level	-13 dB	-16 dB	-15 dB

Chapter 5. Conclusions and Future Work

The creation of a phased-array antenna was described. It began with an assessment of the requirements, which influenced the design. The step-by-step design process using computer simulations was described. The design was then implemented in a manufactured product, which was tested against the requirements and simulated antenna characteristics. The key metrics (beam direction, width, side-lobe levels, gain, and polarization) have all been measured. Beam width, gain and polarization was determined to show good agreement with the simulations and they meet the requirements for the radar system.

The beam direction was 1.5° less than expected from the simulation. The manufacturing errors arising from variations in TL width, adhesive thickness and PCB permittivity explain about 1° of this error. The rest may be due to inherent simulation errors in the software and also measurement alignment error. Similarly, side lobe levels were up to 2 dB higher than expected. Manufacturing errors may account up to 1.5 dB of this deviation, with the remaining error arising from the software or from reflections during the measurements. The beam width increased by about 1° from that of the design. This was not observed in the simulations of manufacturing errors, and may be due to error in the modeling software or reflections. The gain measurements agreed quite well with the simulations. Manufacturing errors seemed to have almost no effect on the gain.

In addition, the weight of a new antenna is less than 15% of the original broad-side antennas (0.4 kg vs. 3 kg), which for 6 antennas will reduce the total weight of the system by more than 15 kg or 25%.

In conclusion, it has been demonstrated that conformal phased-array antennas can replace the current mechanically-oriented antennas for cost saving and further miniaturization of the radar

system. Satisfactory curvature could be achieved by post-manufacture bending, which did not affect the radiation characteristics beyond measurement errors.

5.1 Future Work

In order to make interferometric images and to fully replace the current antennas, a total of 6 antennas need to be manufactured. When funding is available, the following key points should be evaluated and the design updated.

5.1.1 Beam Pattern

The measured main beam direction differed slightly from the simulated one. This should be taken into account if new antennas are to be manufactured. Also, the change in beam direction with frequency should be minimized. With the design, this would be possible either by modifying the TL to have a uniform electrical length across the bandwidth, or by designing two different antennas that are both tuned to the frequency range of only one of the radars, reducing the bandwidth requirement from 200 MHz to 80 MHz. In addition, the radar system itself may be upgraded to use the same frequency band for both forward and aft looking radars. This would reduce the number of transceivers from two to one at the expense of having to add a low-frequency switch to ensure the two radars are not on at the same time. If this is implemented, the antennas would also only need an 80 MHz bandwidth, through which the beam direction change may be acceptable without additional tuning of the TL.

5.1.2 Dual-Beam Layout

The antenna length was already reduced from the ideal 0.61 m to 0.56 m for manufacturing cost savings at the expense of increased beam width. Having six of these antennas next to one another along an aircraft fuselage would need a space of 3.4 m; a quite undesirable requirement. Since only three antennas are needed for along-track interferometry to be next to one another, an obvious

solution is to have the forward and aft looking radar antennas positioned one below the other. This way, the fuselage length would need only to be 1.7 m. If, however, the antennas are positioned in this manner, a natural solution would be to manufacture the forward and aft looking antennas on a single panel (Figure 5.1). The separation between the two antennas would need to be considered for interference as well as the fact the elevation beam direction would change on the curved surface for both. This could be countered by phase-directing the beam in the elevation plane by moving the input of the power divider up or down. On the other hand, if the curvature is small enough, the large elevation beam width may make phasing in the elevation plane unnecessary.

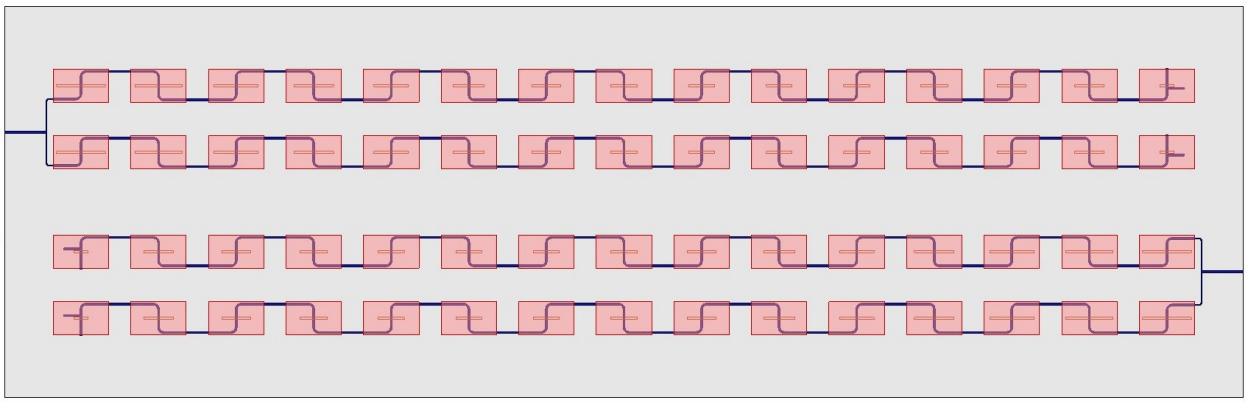

Figure 5.1: Layout of a dual-beam design

5.1.3 Connection

The connectors proved to be too fragile. Having to expose the signal line required to have a 20 mil thick section of a PCB layer support an entire connector against mechanical impacts. The following list provides several different options to make the connection more robust either by itself, or by a combination of some of these improvements:

- Reducing the length of the connector would result in a shorter lever arm through which torque is applied.
- Using a flexible connector would allow much less force to be transmitted down the cable.

- Adding a non-conducting epoxy material around the soldering (after the panel is bent) would greatly strengthen the connection.
- Designing and manufacturing a rigid connector which is clamped onto the board would probably provide the best solution. The connector, however, would need to take the curvature of the board into account, and holes would need be added through the layers for fastening.

5.1.4 Flexibility

The antennas turned out to be much less flexible than it had originally been expected. It is conjectured that the extra rigidity came from the lamination process. Ideally, the antennas should be bendable by hand around an aircraft fuselage and kept in place by clamps or screws. One of the reasons why the antennas required mechanical force to be bent was their relatively low width resulting in a short lever arm. The dual-beam layout would increase this length by a factor of 2, but an even wider panel size may be required for easier bending. Another approach would be to laminate the layers together in a pre-bent configuration. It is yet to be determined whether manufacturers are able to do this and at what extra cost. Lastly, using the edge-press with the large-diameter die to bend the flat antennas also works as demonstrated, so long as the overbending required to achieve the desired curvature does not exceed the sheer limits of the layers.

Appendix A. Dielectric Constant Measurements

The HDPE material considered for cover causes attenuation and frequency shift in the antenna. To model this in software, the dielectric constant had to be determined at the antenna operating frequencies.

The experiment setup consisted of two Vivaldi antennas connected to a NWA facing each other with the sample material between them. The transmission coefficient was measured, from which the phase shift and the dielectric constant was calculated.

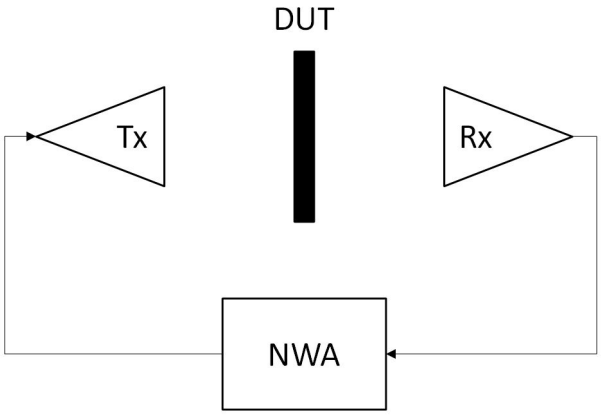

Figure A.1: Experimental setup for dielectric constant measurement

Two different materials were used in the measurement to increase confidence in the validity of the results. In addition to the HDPE sheet, the permittivity of a 1" (2.54 cm) thick polystyrene foam was also measured. It is a very low dielectric constant material, with $\varepsilon_r^{Polystyrene} \approx 1.05$. In comparison, the expected value for the HDPE sheet is $\varepsilon_r^{HDPE} \approx 2.3$.

A.1 Simple Transmission Approximation

As an initial approximation to what phase shift is expected, a single transmission model is used ignoring reflections within the material. The phase of the wave arriving at the receiving antenna is proportional to the wave number and the distance traveled. In air, this means

$$\Theta_1 = -k_0 \cdot L \tag{A.1}$$

With the sample material of thickness D between them, the phase is now given by

$$\Theta_2 = -k_0 \cdot (L - D) - k_0 \cdot \sqrt{\varepsilon_r} \cdot D \tag{A.2}$$

The phase shift introduced by the material is then

$$\Theta_2 - \Theta_1 = k_0 \cdot D \cdot (1 - \sqrt{\varepsilon_r}) \tag{A.3}$$

Using this equation, the expected phase shifts of the polystyrene and the HDPE sheets were plotted as a function of frequency in Figure A.2.

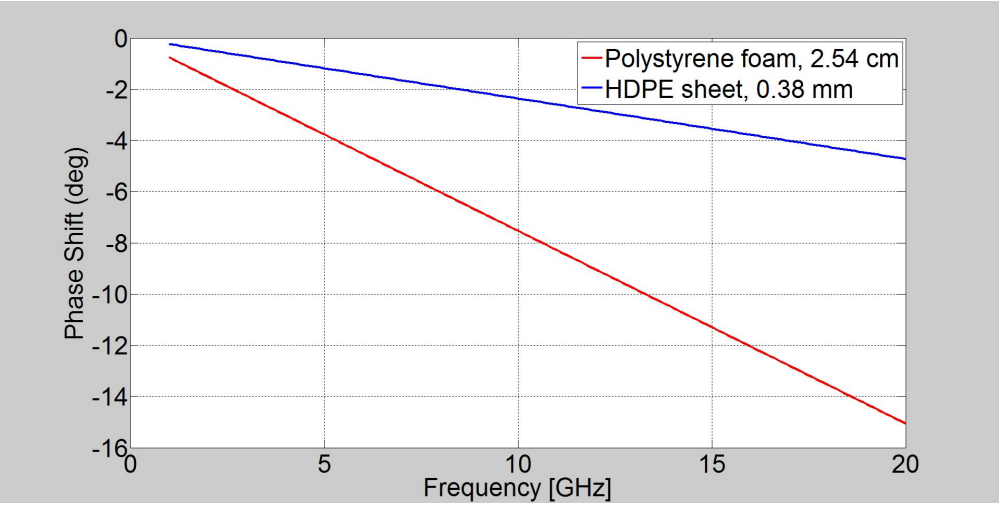

Figure A.2: Estimated phase shifts of the polystyrene foam and HDPE sheet

From the above figure it can be seen that the phase shift will be rather small around the 5 GHz

frequency at which the antenna will operate. In order to decrease the uncertainty in the measured phase shift, it was therefore decided to take the measurements in the 5-15 GHz and 10-20 GHz ranges. The dielectric constant at around 5 GHz was then to be extrapolated from the results. In the experiment, the antennas were also placed at a sufficient distance apart to satisfy the far field condition at these frequencies.

The S_{21} data was then measured with the NWA, and the phase of S_{21} plotted against the frequency. A best linear fit was applied through MATLAB to the resulting plots, which yielded the following revised values: $\varepsilon_r^{Polystyrene} \approx 1.029$, and $\varepsilon_r^{HDPE} \approx 2.65$. Figure A.3 shows the measured and expected phase shifts for an estimated permittivity value of the HDPE material in the 10-20 GHz range.

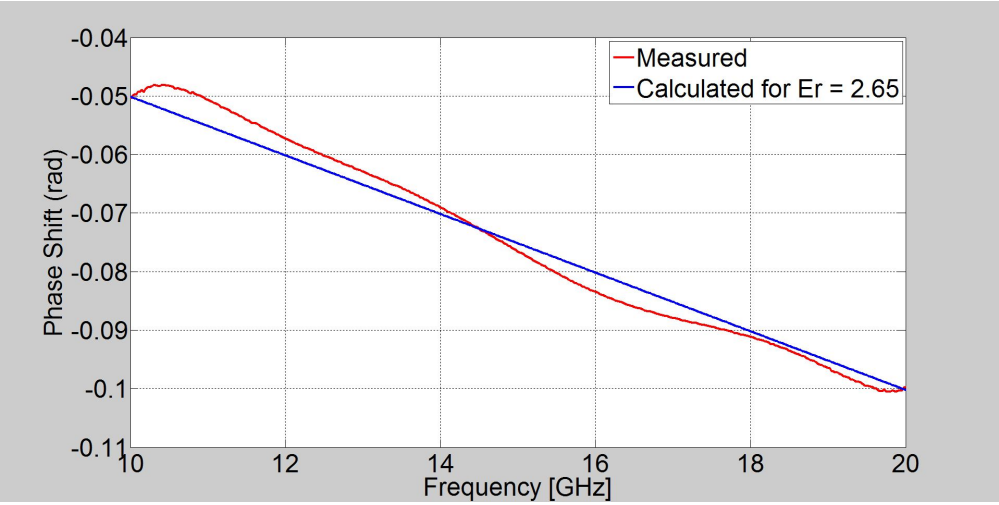

Figure A.3: Measured and calculated S_{21} phase shifts of the HDPE sheet

These approximate values for the dielectric constants were reasonable with the expected values confirming that no major error had been made in the experimental setup and the measured transmission coefficients.

A.2 Multiple Reflection Calculation

For a more accurate relationship between the transmission coefficient and the dielectric constant, the reflections inside the test material need to be taken into account. When an electromagnetic

wave encounters a boundary surface it is split into a transmitted and reflected wave. This reflected wave is bouncing back and forth inside the material adding to the total forward-transmitted wave at every other reflection as illustrated in Figure A.4. (The back-transmitted waves contribute to the total reflected wave from the dielectric.)

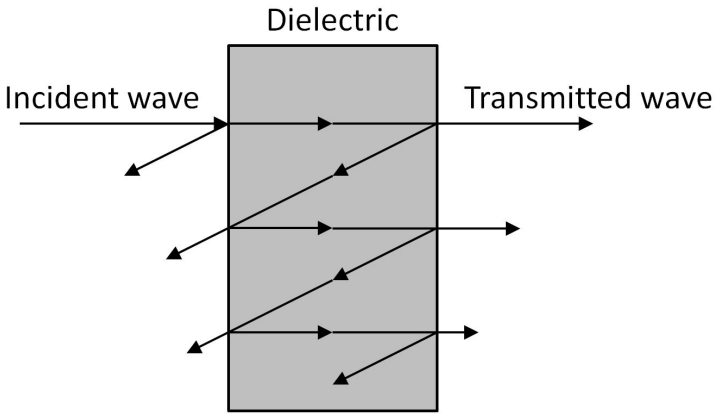

Figure A.4: Multiple reflections inside a dielectric

The total transmitted signal can be calculated as an infinite sum as follows*:

- The phase shift due to the material is given by $e^{-j\Theta} = e^{-jk_r D}$, where $k_r = k_0\sqrt{\varepsilon_r}$ and $k_0 = \frac{2\pi f}{c}$,
- The transmission coefficient from medium m to medium n is denoted as T_{nm},
- Γ is the reflection coefficient at the material boundary, and $\Gamma = \frac{1-\sqrt{\varepsilon_r}}{1+\sqrt{\varepsilon_r}}$,

The total transmitted signal is then given by

$$\begin{aligned} T_{out} &= T_{21}e^{-j\Theta}T_{12} + \\ &\quad T_{21}e^{-j\Theta}\Gamma e^{-j\Theta}\Gamma e^{-j\Theta}T_{12} + \\ &\quad T_{21}e^{-j\Theta}(\Gamma e^{-j\Theta}\Gamma e^{-j\Theta})(\Gamma e^{-j\Theta}\Gamma e^{-j\Theta})T_{12} + \ldots \\ &= T_{21}T_{12}e^{-j\Theta}(1+\Gamma^2 e^{-2j\Theta} + \Gamma^4 e^{-4j\Theta} + \ldots) \\ &= T_{21}T_{12}e^{-j\Theta}\frac{1}{1-\Gamma^2 e^{-2j\Theta}} \\ &= \frac{(1-\Gamma^2)e^{-j\Theta}}{1-\Gamma^2 e^{-2j\Theta}} \end{aligned} \tag{A.4}$$

*Based on lecture notes of Prof. Kuga

From this, the measured transmission coefficient at the NWA can be expressed as follows

$$S_{21} = \frac{(1-\Gamma^2)e^{-jk_rD}}{1-\Gamma^2 e^{-2jk_rD}} e^{jk_0D} \tag{A.5}$$

Since S_{21} was measured as a function of f, the equation had to be solved numerically for ε_r. To this end, the MATLAB *fminsearch* function was used. Also, in order to reduce random error in the experiments, the transmission coefficient of the HDPE sheet was measured four times for each frequency range. Figures A.5 and A.6 show the real and imaginary parts of the calculated permittivity for the four different measurements in both frequency ranges. The measurement is expected to be more reliable in the center region than the outer edges due to averaging. Nevertheless, the dielectric constant seems to depend sinusoidally on the frequency and the variation in the imaginary part is quite large. Trying to extrapolate from these results to 5 GHz would give too much uncertainty in ε_r. Because of this, using the HDPE material as cover for the antennas was abandoned in favor of a costlier material with known precise electric qualities.

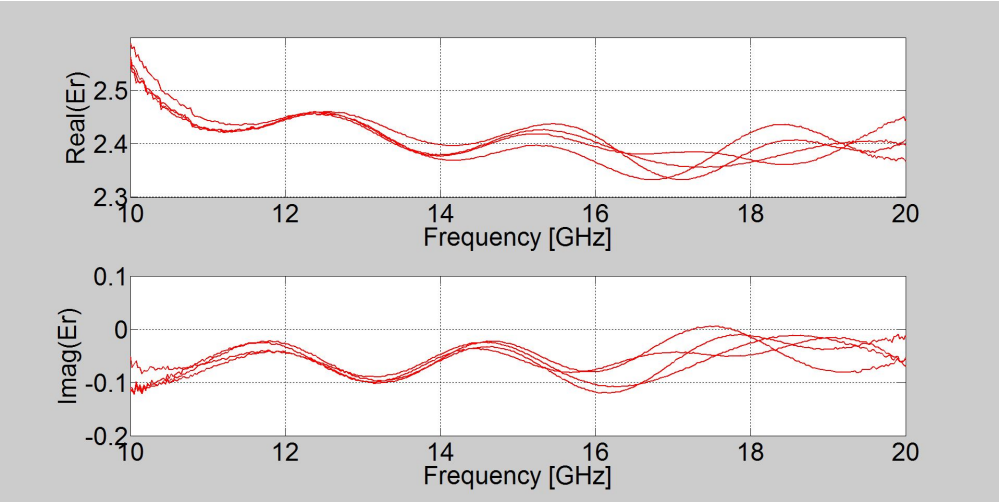

Figure A.5: Calculated real and imaginary parts of ε_r for the HDPE sheet at 10-20 GHz

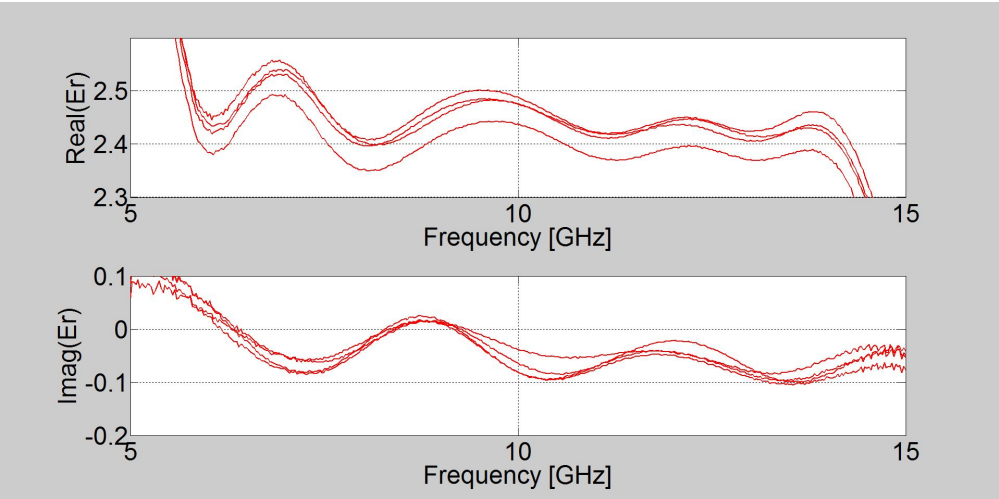

Figure A.6: Calculated real and imaginary parts of ε_r for the HDPE sheet at 5-15 GHz

Appendix B. Pictures of the Test Equipment

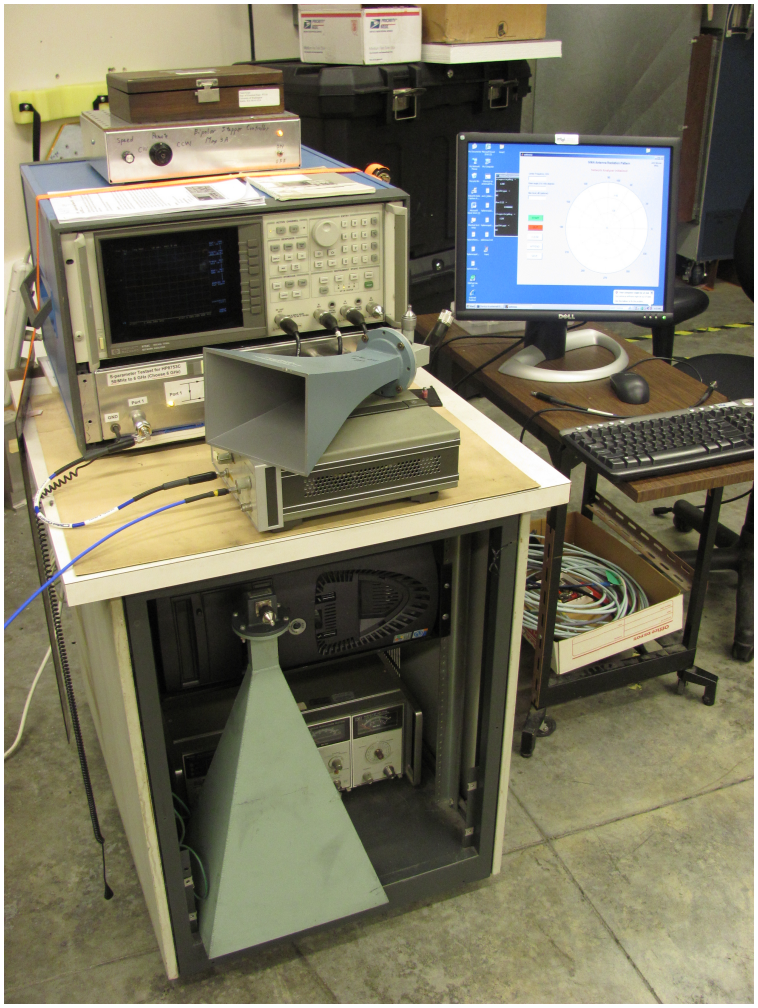

Figure B.1: NWA, PC, amplifier, and standard gain horn antenna

Figure B.2: Total station used to align the AUT

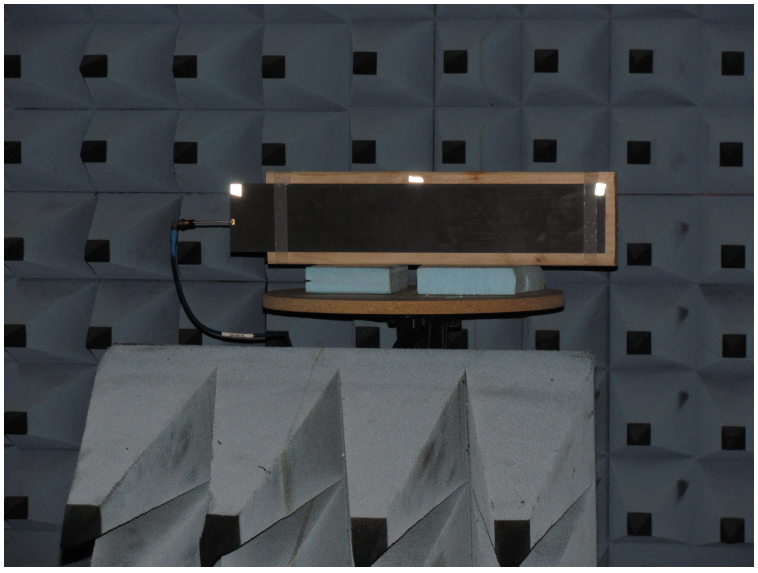

Figure B.3: AUT in the anechoic chamber with reflectors for alignment with the total station

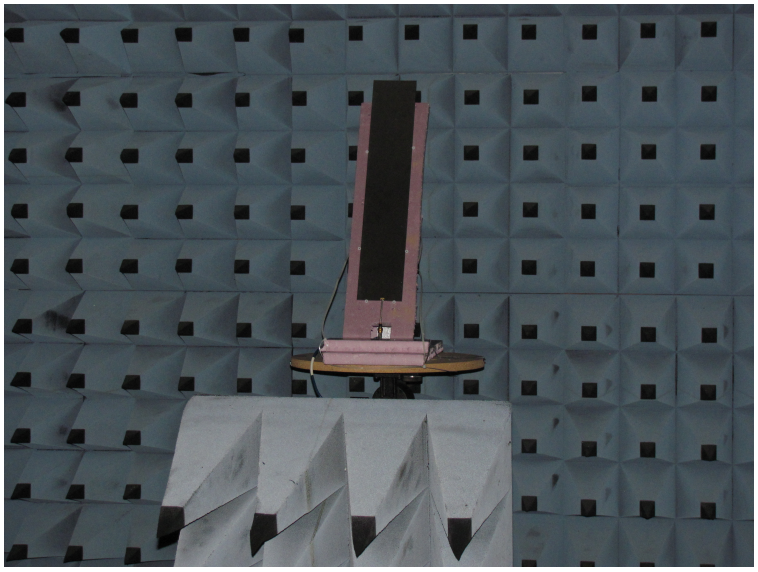

Figure B.4: AUT in vertical position to measure beam-plane pattern

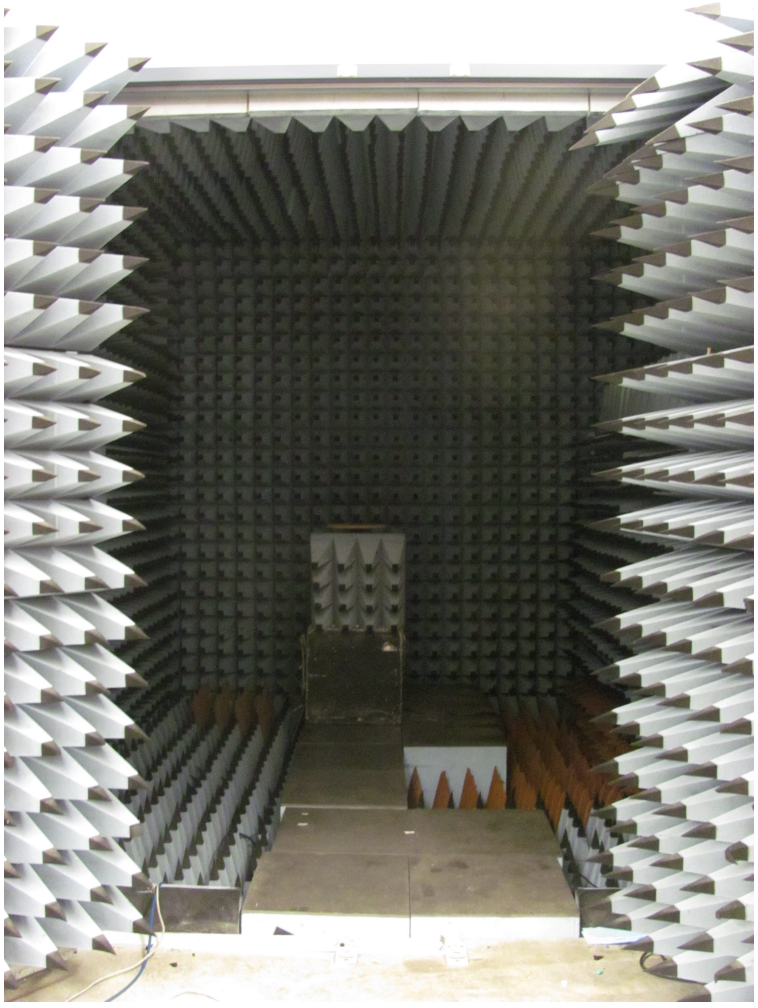

Figure B.5: Anechoic chamber where the AUT was placed

Figure B.6: Vivaldi Tx antenna

Appendix C. Figures of the Measured Radiation Patterns

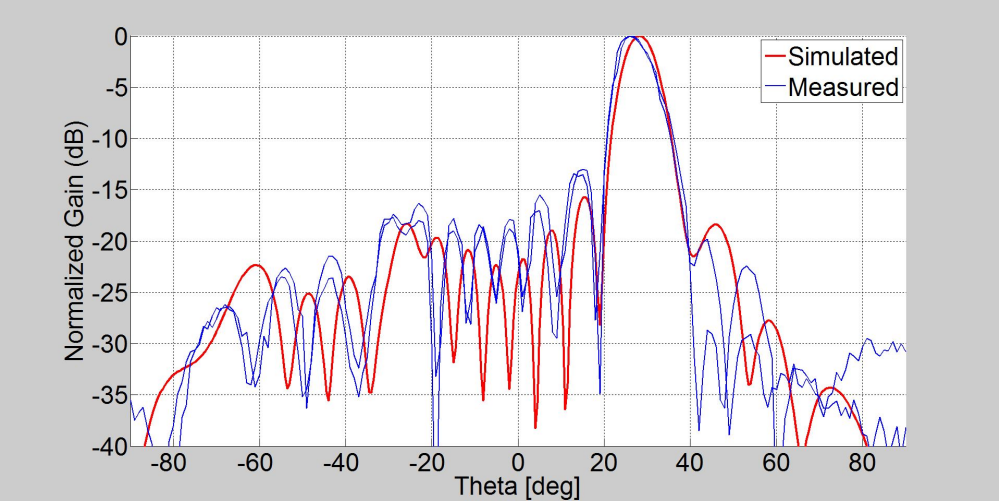

Figure C.1: Simulated vs. measured radiation patterns at 5.33 GHz

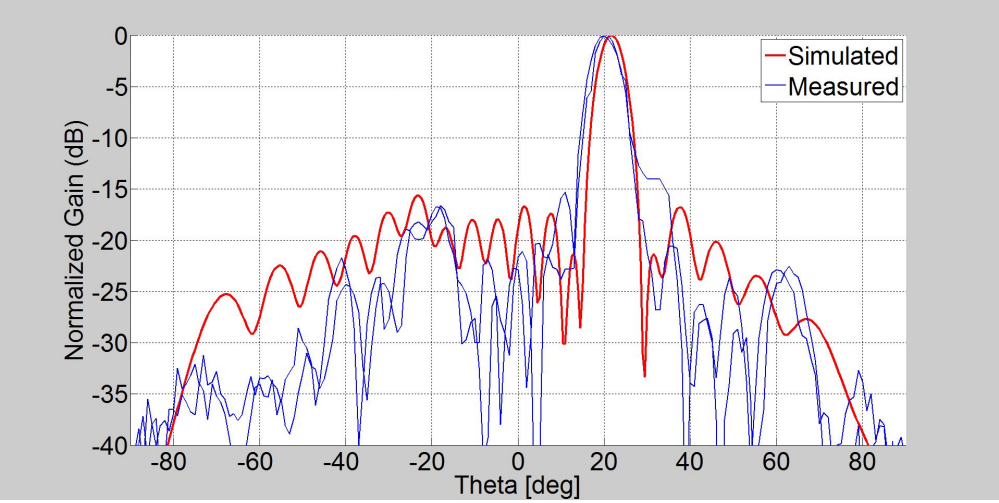

Figure C.2: Simulated vs. measured radiation patterns at 5.53 GHz

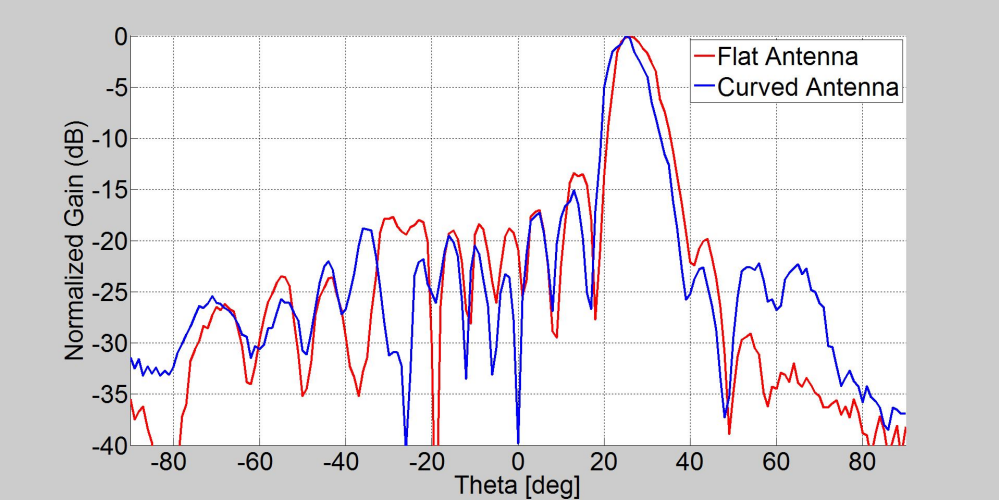

Figure C.3: Flat vs. conformal antenna H-plane radiation patterns at 5.33 GHz

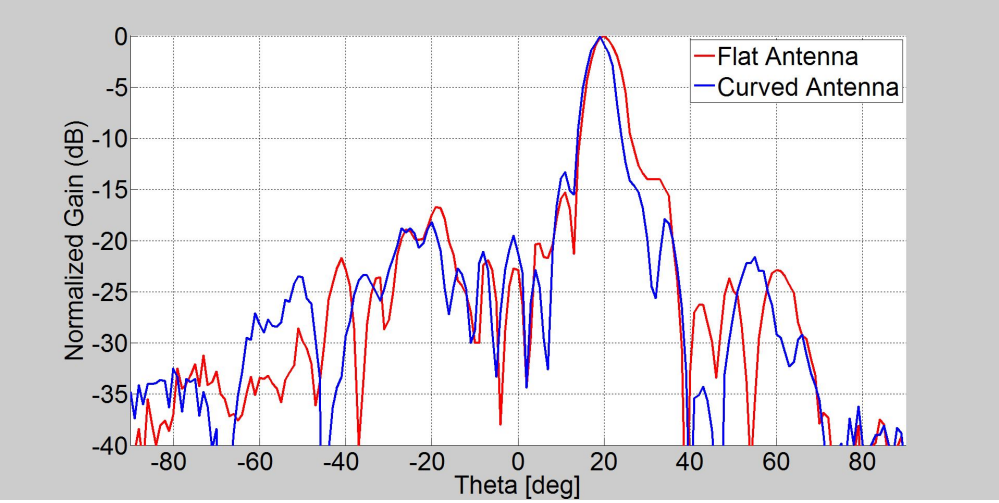

Figure C.4: Flat vs. conformal antenna H-plane radiation patterns at 5.53 GHz

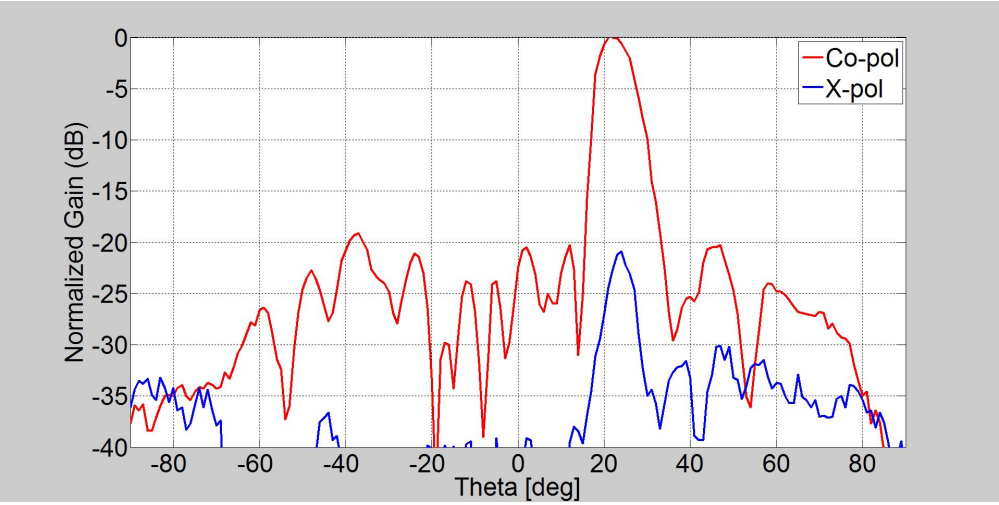

Figure C.5: Measured H-plane co- and cross-polarization radiation patterns at 5.43 GHz

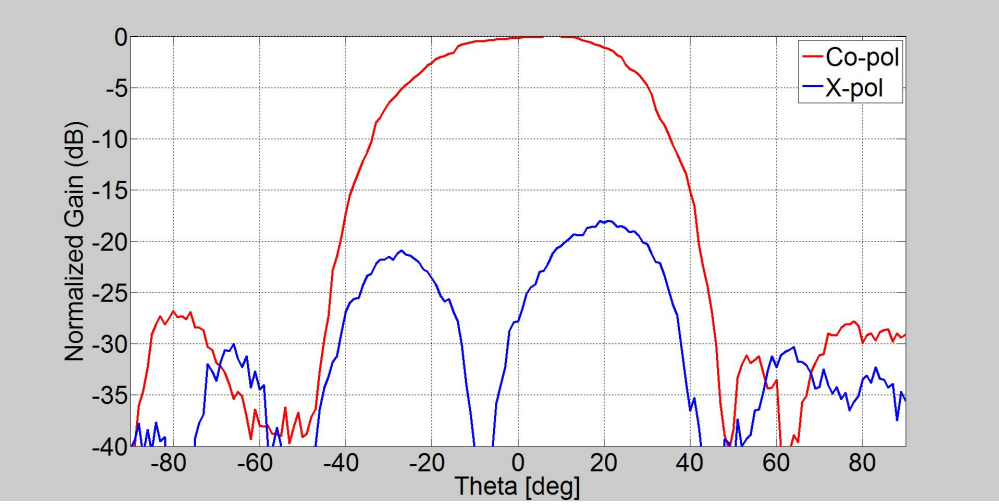

Figure C.6: Measured beam-plane co- and cross-polarization radiation patterns at 5.43 GHz

Glossary of Acronyms

ACPA	aperture-coupled patch antenna
AUT	antenna under test
CAD	computer-aided design
CW	continuous wave
DUT	dielectric under test
EMCPA	electromagnetically-coupled patch antenna
FMCW	frequency-modulated continuous wave
GND	ground
HDPE	high-density polyethylene
INS	inertial navigation system
MSAA	microstrip array antenna
NWA	network analyzer
PCB	printed circuit board
PRR	pulse repetition rate
Rx	receiver / receiving
SAR	synthetic aperture radar
SNR	signal-to-noise ratio
TL	transmission line
Tx	transmitter / transmitting
UAV	unmanned aerial vehicle

Bibliography

[1] T. Elfouhaily, B. Chapron, K. Katsaros: "A Unified Directional Spectrum for Long and Short Wind-driven Waves", *Journal of Geophysical Research*, vol. 102, no. C7, pp. 15,781-15,796, July 1997

[2] S. J. Frasier, A. J. Camps: "Dual-Beam Interferometry for Ocean Surface Current Vector Mapping", *IEEE Transactions on Geoscience and Remote Sensing*, vol. 39, no. 2, pp. 401-414, February 2001

[3] G. Farquharson, W. N. Junek, A. Ramanathan, S. J. Frasier, R. Tessier, D. J. McLaughlin, M. A. Sletten, J. V. Toporkov: "A Pod-Based Dual-Beam SAR", *IEEE Geoscience and Remote Sensing Letters*, vol. 1, no. 2, pp. 62-65, April 2004

[4] F. T. Ulaby, R. K. Moore, A. K. Fung: *Microwave Remote Sensing, Volume II*, Artech House Microwave Library, Boston, MA, 1986

[5] W. J. Plant: "Bragg Scattering of Electromagnetic Waves from the Air/Sea Interface", *Surface Waves and Fluxes, Volume II - Remote Sensing*, Kluwer Academic Publishers, Norwell, MA pp. 41-108, 1990

[6] D. M. Pozar: *Microwave Engineering*, John Wiley & Sons, Inc., NJ, 1980

[7] D. M. Pozar: "Microstrip antennas", *IEEE Proc.*, vol. 80, pp. 79-91, January 1992

[8] C. A. Balanis: *Antenna Theory - Analysis and Design*, John Wiley & Sons, Inc., NJ, 3rd Edition, 2005

[9] W. L. Stutzman, G. A. Thiele: *Antenna Theory and Design*, John Wiley & Sons, Inc., NJ, 3rd Edition, 2012

[10] D. M. Pozar, B. Kaufman: "Increasing the bandwidth of a microstrip antenna by proximity coupling", *Electronic Letters*, vol. 23, no. 8, pp. 368-369, April 9 1987

[11] M. Stoneback, M. Stoneback, Y. Kuga: "Feasibility Study of a Wirelessly Controlled and Powered Space-Fed Phased Array Antenna", *IEEE Transactions on Antennas and Propagation*, vol. 61, no. 12, pp. 5984-5991, December 2013

[12] D. M. Pozar: "Microstrip antenna aperture-coupled to a microstripline", *Electronic Letters*, vol. 21, no. 2, pp. 49-50, January 17 1985

[13] D. M. Pozar: "Analysis and Design of Cavity-Coupled Microstrip Couplers and Transitions", *IEEE Transactions on Microwave Theory and Techniques*, vol. 51, no. 3, pp. 1034-1044, March 2003

[14] D. M. Pozar: "A Review of Aperture Coupled Microstrip Antennas: History, Operation, Development, and Applications", University of Massachusetts at Amherst, May 1996

[15] M. P. Civerolo: "Aperture Coupled Microstrip Antenna Design and Analysis", Thesis, California Polytechnic State University, 2010

[16] A. Kuchar: "Aperture-Coupled Microstrip Patch Antenna Array", Thesis, Technische Universität Wien, 1996

[17] J. L. Salazar, R. Medina, E. J. Knapp, D. J. McLaughlin: "Phase-Tilt Array Antenna Design for Dense Distributed Radar Networks for Weather Sensing", *Proceedings of IGARSS 2008*, vol. 5, pp. 318-321, July 2008

[18] L. Josefsson, P. Persson: *Conformal Array Antenna Theory and Design*, Wiley-IEEE Press, 2006

[19] P. Knott, T. Bertuch, H. Wilden, O. Peters, A. R. Brenner, I. Walterscheid: "SAR Experiments Using a Conformal Antenna Array Radar Demonstrator", *International Journal of Antennas and Propagation*, 2012

[20] C. Ahn, Y. Ren, K. Chang: "A Dual-Polarized Cylindrical Conformal Array Antenna Suitable for Unmanned Aerial Vehicles", *International Journal of RF and Microwave Computer-Aided Engineering*, vol. 21, issue 1, pp. 91-98, January 2011

[21] R. Garg, I. Bahl, M. Bozzi: *Microstrip Lines and Slotlines*, Artech House Microwave Library, Boston, MA, 3rd Edition, 2013